

# MIRA: Cracking Black-box Watermarking on Deep Neural Networks via Model Inversion-based Removal Attacks

Yifan Lu, Wenxuan Li, Mi Zhang, Xudong Pan, Min Yang  
Fudan University, China

{luyf23@m., liwx22@m., mi\_zhang@, xdpan@, m\_yang@}fudan.edu.cn

## Abstract

To protect the intellectual property of well-trained deep neural networks (DNNs), black-box DNN watermarks, which are embedded into the prediction behavior of DNN models on a set of specially-crafted samples, have gained increasing popularity in both academy and industry. Watermark robustness is usually implemented against attackers who steal the protected model and obfuscate its parameters for watermark removal. Recent studies empirically prove the robustness of most black-box watermarking schemes against known removal attempts.

In this paper, we propose a novel Model Inversion-based Removal Attack (MIRA), which is watermark-agnostic and effective against most of mainstream black-box DNN watermarking schemes. In general, our attack pipeline exploits the internals of the protected model to recover and unlearn the watermark message. We further design target class detection and recovered sample splitting algorithms to reduce the utility loss caused by MIRA and achieve data-free watermark removal on half of the watermarking schemes. We conduct comprehensive evaluation of MIRA against ten mainstream black-box watermarks on three benchmark datasets and DNN architectures. Compared with six baseline removal attacks, MIRA achieves strong watermark removal effects on the covered watermarks, preserving at least 90% of the stolen model utility, under more relaxed or even no assumptions on the dataset availability.

## 1 Introduction

In recent years, deep neural networks (DNNs) are empowering real-world applications in computer vision [42, 57], natural language processing [15, 20], and autonomous driving [5, 6]. However, training a modern DNN from scratch requires time-consuming data collection and high-end computing resources. To protect the intellectual property of well-trained DNNs, *model watermarking* is an emerging tool for verifying the ownership of DNNs in case of model stealing.

Generally, in a DNN watermarking scheme, the secret watermark information is embedded into the *target model* at the

Table 1: Our attack effectively removes most of the mainstream black-box watermarks in an S&P’22 SoK paper on DNN watermarking [39]) from protected DNN models, when the utility is preserved at an acceptable level.

| Targets        | Prune [37, 48] | Finetune [8, 43, 58] | Unlearning [4] | MIRA |
|----------------|----------------|----------------------|----------------|------|
| Content [56]   | ✓              | ✓                    | ✓              | ✓    |
| Noise [56]     | ✗              | ✗                    | ✗              | ✓    |
| Unrelated [56] | ✓              | ✓                    | ✗              | ✓    |
| Piracy [34]    | ✗              | ✓                    | ✗              | ✓    |
| EWE [25]       | ✗              | ✗                    | ✗              | ✓    |
| Adi [3]        | ✗              | ✓                    | ✗              | ✓    |
| AFS [29]       | ✗              | ✗                    | ✗              | ✓    |
| EW [41]        | ✗              | ✗                    | ✗              | ✓    |
| Blind [36]     | ✗              | ✗                    | ✗              | ✓    |
| Mark [18]      | ✗              | ✓                    | ✗              | ✓    |

watermark embedding stage during training. At the verification stage, the watermark is extracted from the *suspect model* to determine its ownership. Depending on how the suspect model is accessed during verification, current watermark algorithms can be categorized into *white-box* and *black-box* watermarks. A white-box watermark is usually embedded into the suspect model’s internal information, i.e., model parameters [10, 48, 51] or neuron activation [14]. In comparison, a black-box watermark is embedded into a model’s prediction behaviour on a set of specially-crafted samples (i.e., *watermark data*) by specifying their expected classification results (i.e., *target classes*). Owing to the weaker access requirement, black-box watermarks have gained increasing popularity in both academy and industry, with commercial applications (e.g., IBM [2]).

Considering its application prospects, recent studies systematically evaluate the robustness of black-box model [33, 39] against *watermark removal attacks*, which modifies the model parameters to cause verification failure. According to Wang et al. [46], existing removal attacks are mainly categorized into three types, pruning-based, finetuning-based and unlearning-based. Unfortunately, as shown in Table 1, they can only crack a subset of black-box watermarks (i.e., significantly lowering the watermark verification success rate, with most of the utility preserved). To be more specific, these

attacks may to varied degrees hamper the model’s utility, remove the watermark incompletely, require certain prior knowledge of the target watermark, or have a strong dependence on the original training data [8, 19, 39, 58]. A general comparison of their attack budgets is summarized in Table 2 and a more detailed analysis is presented in Section 2. With more robust black-box watermarks recently proposed [25, 29, 41], the robustness of black box DNN watermarks seems to be guaranteed.

**Our Work.** In this paper, we propose a novel **Model Inversion-based Removal Attack** (dubbed as MIRA), which is watermark-agnostic and cracks ten existing black-box DNN watermarks with almost no dependence on the dataset availability (Table 1). Our insights are based on the commonality of existing black-box watermarks, which leverages the over-parameterization property of DNN models to additionally memorize watermark data correlated to the target labels. This mechanism means that the model internally store the watermark information, which the attacker can exploit to **recover and unlearn** the watermark data from the protected model.

Technically, we design a general-purpose two-stage watermark removal framework. At the first stage, we use an aggressive model inversion technique to reverse-engineer class-wise samples close to the real watermark data from a target watermarked model (§4.1). This recovering method is especially powerful, compared to existing trigger reverse-engineering or general inversion methods. At the second stage, we specially unlearn these samples during the finetuning process (§4.2). This basic MIRA framework is effective against almost all the mainstream black-box watermarks. However the basic MIRA may affect the model’s utility mainly because a small proportion of the recovered samples can be irrelevant to the underlying watermark or contain information critical to the main task.

To address this issue, we further enhance MIRA in the following directions. First, we improve the recovering stage of MIRA via incorporating target class detection. For watermarks with fixed target classes (such as [56] and [25], where all the watermark data are paired with the identical target class), we derive an observation called *watermark smoothness* that, the loss landscape of model is smoother with respect to samples of the target class, compared to samples of other classes. We leverage the difference in smoothness to distinguish whether the target watermark has a fixed target class, and, if so, detect its target class. This allows us to only recover the samples belonging to the target class when cracking a fixed-class watermark (§5.1). Next, we improve the unlearning stage of MIRA via splitting recovered samples. Our improvements are based on the observed *normal data dominance*, i.e., the normal data tend to occupy a larger space than the watermark data in the watermarked model’s decision region. Therefore, we combine this with salient neuron analysis on the recovered samples and carefully split them into proxy watermark data and proxy normal data. The split recovered samples are

fed into the final fine-tuning process to enhance the removal specificity and mitigate the impact on utility (§5.2).

With the above improvements, MIRA is watermark-agnostic and generally effective, with little impact on the utility. Moreover, the split proxy normal data can even allow for a data-free removal attack for watermarks identified with fixed target classes. Table 2 summarizes the advantages of our attack compared with existing removal attempts.

**Our Contribution.** We summarize the key contributions of this work as follows:

- By summarizing the commonality of existing black-box DNN watermarks in specially memorizing watermark data correlated to the target labels, we uncover a new removal attack surface via recovering and unlearning watermark samples from a target watermarked model. Our novel attack MIRA is watermark-agnostic and effective against almost all the existing black-box watermarks.
- Based on in-depth analysis and observations on the existing black-box watermark schemes, we further improve the basic MIRA with target label detection and recovered sample splitting algorithms. The improvements help reduce the utility loss caused by MIRA on the target model and relax the dependence on in-distribution/transfer datasets when attacking half of the black-box watermarking schemes.
- We conduct comprehensive evaluation of MIRA against ten mainstream black-box watermarks on three benchmark datasets and DNN architectures, under three different data settings. Compared with six baseline removal attacks, our proposed MIRA is proved more effective in watermark removal and has less impact on the model’s utility, while requiring more relaxed or even no assumptions on the dataset availability. To facilitate future studies, we open-source our code in the following repository: <https://anonymous.4open.science/r/MIRA-07E6>.

## 2 Background

• **Model Watermarks.** Digital watermarking is originally designed for protecting the copyright of digital media [26] and recently applied to protect the intellectual property of DNN models. A white-box watermarking scheme typically embeds a sequence of secret messages into the parameters or neural activations of the target model, and thus requires white-box access of the suspect model to extract the watermark [10, 14, 48, 51]. On the contrary, a black-box watermark is embedded in the model’s prediction behavior on a set of specially-crafted secret samples. Therefore, the verification process of black-box watermarking only requires the access to the prediction API [3, 25, 29, 56]. In this work, we mainly focus on the robustness of black-box watermarks due to their increasing popularity in industry.

Existing black-box watermark schemes have diverse designs in the choices of the *watermark data* and the *target*

*label*. In terms of watermark data, some work leverages specially-crafted patterns [25, 56] or random noise [56] as watermark patterns. Other black-box watermarks may use out-of-distribution samples as watermark data [3, 56]. Besides, in-distribution clean samples [41], adversarial samples near the decision boundary [29] or images generated by an encoder with exclusive logo embedded indistinguishably [36] can also be exploited as watermark data. In terms of the target label setting, existing black-box DNN watermarks can be categorized into fixed-class watermarks, where all the watermark data are paired with the identical target class (such as [25, 34, 56]), and non-fixed-class watermarks, where each watermark data is paired with its own target class (such as [3, 18, 29, 36, 41]).

To build a trustworthy ownership verification process, an ideal watermarking scheme should satisfy the following three key requirements [39, 52]. (1) **Fidelity**. The performance degradation on the target model should be as low as possible after the watermark is embedded. (2) **Integrity**. Models which are trained independently without access to the target model should not be verified as containing the watermark. (3) **Robustness**. The embedded watermark in the target model should be resistant to potential removal attacks. In the extreme settings when the watermark is removed, the utility of the model should decrease dramatically.

- **Watermark Removal Attacks**. Black-box model watermarks are to some extent similar to backdoor attacks, as they both establish connections between some specified data and the target labels. Therefore, classical methods in backdoor defense, such as pruning, finetuning or trigger reverse-engineering, are usually considered as potential threats for black-box watermarks [3, 25, 56]. Recently, some attacks specially targeting black-box watermarks are also proposed.

According to Wang et al. [46], existing watermark removal attacks are mainly categorized into three types as follows.

- **Pruning-based Attacks**: They prune the redundant weights [48] or neurons [37] in DNNs. However, to invalidate the underlying watermarks, these methods need to prune a large proportion of weights or neurons, which causes an unacceptable utility loss.
- **Finetuning-based Attacks**: They continue to train the target model for a few epochs with some carefully designed finetuning techniques, such as learning rate schedule [8, 9], dataset augmentation [38], weight regularization [43], or continue learning with attention distraction [58]. Unfortunately, these attacks are usually effective only against a subset of watermarks, and might hamper the model’s utility due to the heavy training restrictions.
- **Unlearning-based Attacks**: They are mainly designed for black-box watermarks whose watermark data have the fixed pattern and the identical target class [4, 46]. Specifically, they use conventional backdoor trigger reverse-engineering techniques in e.g., *NeuralCleanse* [50], which poses rather strong assumptions on the forms of underlying watermarks

Table 2: Comparison of attack budgets between our attack and existing watermark removal attacks, where ●/◐/○ represent high, medium and low (or no) attack budget.

| Attack Type | Utility Loss | Removal Ineffectiveness | Watermark Knowledge | Dataset Access |
|-------------|--------------|-------------------------|---------------------|----------------|
| Prune       | ◐            | ◐                       | ○                   | ◐              |
| Finetune    | ◐            | ◐                       | ○                   | ●              |
| Unlearn     | ○            | ○                       | ●                   | ●              |
| MIRA        | ○            | ○                       | ○                   | ◐              |

and are therefore not watermark-agnostic. Also, current unlearning-based attacks all need access to source training data, which further limits their applicable scenarios.

Table 2 summarizes the pros-and-cons of attacks from each category. Note that there also exists another type of attacks aiming at training a new surrogate model using the knowledge transferred from the given watermarked model, i.e., model extraction attacks [25, 39, 53]. However, extraction attacks typically requires large query dataset and entails heavy computation costs [43]. Therefore, our current work is not compared with extraction attacks.

Our work focuses on the vulnerabilities revealed by model inversion. Note that this has also been studied by Zhang et al. [56]. However, they used a rather naive inversion method from [16] and only presented the visually-meaningless inverted samples. Neither have they delved into the neuron coverage between the inverted samples and the real watermark samples, nor attempted to unlearn the inverted ones for watermark removal.

### 3 Security Settings

#### 3.1 Mechanism of Black-box Watermarking

The true model owner is denoted as  $O$ . During the training,  $O$  embeds a watermark into the target model by training on both the clean dataset  $X = \{(x_i, y_i)\}_{i=1}^{N_1}$  ( $y_i \in \{0, 1, \dots, C-1\}$ ) from its main task, where  $C$  is the total number of the classification classes, and on a set of specially-crafted watermark data  $X_w = \{(x_{wi}, y_{wi})\}_{i=1}^{N_2}$  ( $y_{wi} \in \{0, 1, \dots, C-1\}$ ), where target classes  $y_{wi}$  can be either identical or sample-specific. We denote the watermarked model as  $f_w$ .

By inspecting the official watermark implementations, we observe the following technical designs which the owner  $O$  will take to meet the three requirements in Section 2. Specifically, to satisfy the **fidelity** purpose,  $O$  usually choose an over-parameterized model with enough capacity, which is trained on both normal samples and watermark samples, with normal ones being dominant in quantity [3, 36], i.e.,  $N_2 \ll N_1$ . To ensure the watermark **integrity**,  $O$  typically crafts watermark samples  $(x_{wi}, y_{wi})$  that are significantly different from the normal samples in the target class  $y_{wi}$ , whose size  $N_2$  cannot be too small as well, to claim the ownership with high

confidence [25, 34, 39]. To enhance the **robustness** of the embedded watermark,  $O$  tends to intentionally increase the involvement of the watermark data in the training process. For instance, both Adi et al. [3] and Lederer et al. [32] concatenate the independently sampled normal data and watermark data into a data batch during each training iteration. Jia et al. [25] intentionally train the model on watermark samples and on normal samples alternatively. Lukas et al. [39] explicitly boost the ratio of watermark data when constructing the total training set in their open-source framework *Watermark-Robustness-Toolbox*<sup>1</sup>.

In face of potential copyright infringement,  $O$  is able to verify the model ownership by checking the suspect model’s predictions on  $X_w$ .

### 3.2 Threat Model

**Attack Scenario.** In our threat model, the attacker  $\mathcal{A}$  has managed to acquire the model  $f_w$  by means of, e.g., compromising  $O$ ’s server or receiving assistance from an insider.  $\mathcal{A}$  has white-box access to observe the parameters of  $f_w$  as well as to modify them, similar to the settings in the recent watermark robustness studies [33, 39].  $\mathcal{A}$  is aware of the existence of the watermark in  $f_w$ , and therefore his/her goal is to derive a surrogate model  $f_a$  from  $f_w$  to fail the ownership verification.

**Attack Budget.** Specifically, as shown in Table 2, ①  $\mathcal{A}$  has no knowledge of the specific watermark algorithm or the watermark data  $X_w$   $O$  used (i.e., watermark-agnostic). ②  $\mathcal{A}$  hopes to significantly lower  $f_a$ ’s watermark verification accuracy on  $X_w$ , ③ while preserving its clean accuracy on the main task. Next, ④  $\mathcal{A}$  wants to relax the dataset access requirement as much as possible.

Previous removal attacks may require a substantial subset of the clean training data  $X$  [3, 8, 56], or a considerable size of unlabeled data collected from open sources as proxy data [19, 43]. However, they usually ignore the difficulty of collecting high-quality data at such a scale. In this work, we mainly consider the attacker with limited data access, as in [4, 58]. The following three assumptions on dataset availability characterizes attackers from being limited in knowledge to almost of zero knowledge:

- **In-distribution:** A limited number of correctly labeled samples (either manually by humans, or automatically by the well-training watermarked model) are available from the same distribution of the target model’s main task. This setting is realistic since these in-distribution data are often hard to acquire.
- **Transfer:** A small amount of unlabeled data from a transfer distribution is available. Note that the distribution of these unlabeled data also matters, since finetuning the target model on samples from a completely different distribution might lead to catastrophic forgetting [27].

- **Data-free:** No additional data is available. This setting further relaxes the dataset access requirement for the attacker. To the best of our knowledge, our work is the first to formally consider data-free black-box watermark removal settings.

## 4 General Framework of MIRA

In general, our MIRA adopts the following two-stage attack pipeline: a) **Watermark Recovering:** We first leverage model inversion technique to recover some samples close to real watermark data (§4.1). b) **Watermark Unlearning:** We next deliberately unlearn these samples during the fine-tuning process, along with the auxiliary dataset  $\mathcal{A}$  possesses §4.2). An overview of our general attack framework is shown in the upper region of Fig. 1.

### 4.1 Watermark Recovering

Despite the complexity of various underlying forms of watermarks, including different watermark patterns and strategies for setting the target labels of the watermark data, we summarize their commonality in exploiting the over-parameteration property of DNNs to specially memorize the watermark data correlated to the pre-defined target labels. To put it another way, the watermark information is implicitly stored in the watermarked models. In this way, we attempt to use model inversion techniques to reverse-engineer samples close to the real watermark data from a watermarked model.

Concretely, we use optimization-based model inversion to recover the samples hidden in the watermarked model  $f_w$ . Given a target class  $c$  and a batch of randomly initialized samples  $B = \{\hat{x}_i\}_{i=0}^{M-1}$  ( $\hat{x}_i$  keeps the same shape as the images of  $f_w$ ’s main task, while  $M$  is the number of samples to be optimized for the  $c$ -th class, we try to reverse-engineer samples which are similar to the watermark data correlated to the target class  $c$  by optimizing

$$\min_B \left( \sum_{\hat{x}_i \in B} \mathcal{L}(f_w(\hat{x}_i), c) \right) + \mathcal{R}(B), \quad (1)$$

where  $\mathcal{L}(\cdot)$  is the cross-entropy loss, and the regularizer  $\mathcal{R}(\cdot)$  poses our prior knowledge on the watermark data.

In addition to classic priors on natural images (e.g.,  $\ell_2$  regularization and total variation regularization [40]), our recovering algorithm mainly exploits the information stored in the batch normalization (BN) layers [24], as is done in [54, 55]. BN layers are widely adopted in mainstream DNNs [21, 22, 47], and keep useful statistics of the training data, capturing both low-level and high-level features in the neural network. Since the owner  $O$  tends to intentionally increase the involvement of the watermark data during the training, for the robustness purpose described in Section 3.1, the watermark data  $X_w$  are expected to play an important role in the BN statistics of the target model  $f_w$ .

<sup>1</sup> <https://github.com/dnn-security/Watermark-Robustness-Toolbox>



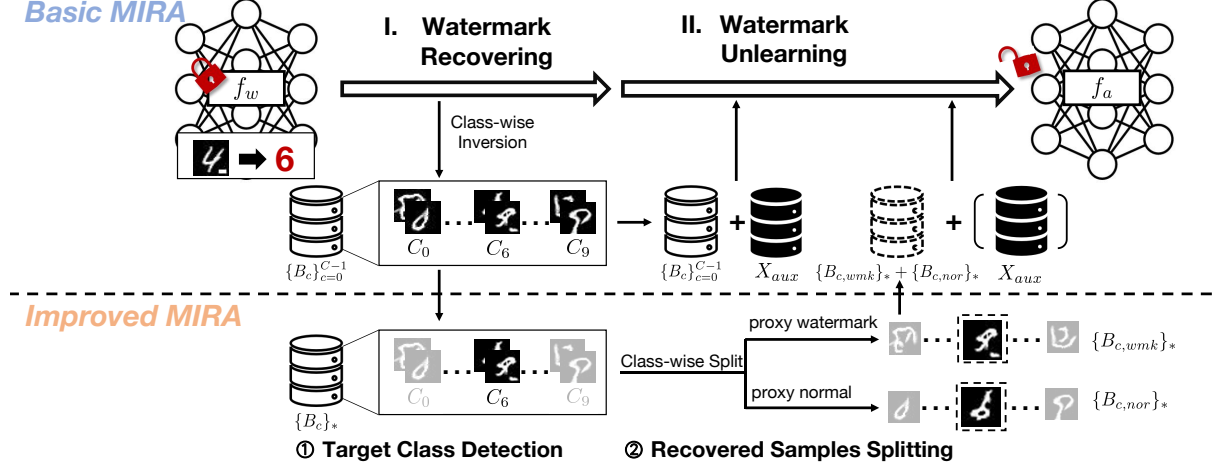


Figure 1: **The overview of our MIRA.** The upper region shows our **basic MIRA**, which consists of two stages, watermark recovering (§4.1) and watermark unlearning (§4.2). The lower region represents our **improved MIRA**, which detects the possible target class of the underlying watermark after recovering (§5.1), and identifies samples more relevant to the real watermark data before unlearning (§5.2).

To better utilize the watermark information hidden in the BN layers, we employ another feature distribution regularization term  $\mathcal{R}_{bn}(\cdot)$  to guide the recovered samples closer to the real watermark data:

$$\mathcal{R}_{bn}(B) = \sum_{l=0}^{L-3} \|\mu_l(B) - \mu_l\|_2^2 + \|\sigma_l^2(B) - \sigma_l^2\|_2^2, \quad (2)$$

where  $L$  is the total number of BN layers in  $f_w$ ,  $\mu_l$  and  $\sigma_l^2$  are the running batch-wise mean and variance stored in the  $l$ -th BN layer, while  $\mu_l(\cdot)$  and  $\sigma_l^2(\cdot)$  are current statistics of feature maps before the  $l$ -th BN layer. According to [23, 44], the last several layers of DNN captures the high-level features, which is more correlated with the model’s prediction behavior. Therefore, in the above BN regularization, we intentionally dismiss the guidance of the last two BN layers. This design prevents the recovered samples from being pulled towards the center of all classes in high-level decision space, and encourages them to explore more space in class  $c$ ’s decision region.

In summary, the regularization term in Equation 1 is finally designed as:

$$\mathcal{R}(B) = \alpha_{\ell_2} \mathcal{R}_{\ell_2}(B) + \alpha_{tv} \mathcal{R}_{tv}(B) + \alpha_{bn} \mathcal{R}_{bn}(B), \quad (3)$$

where  $\mathcal{R}_{\ell_2}(B)$  and  $\mathcal{R}_{tv}(B)$  penalize the  $\ell_2$  norm and the total variation of the recovered watermark data. The detailed forms can be found in Appendix A.1.

As is set up in Section 3.2, the attacker  $\mathcal{A}$  has no knowledge of the target watermark form and is therefore unaware of the target label  $c$  associated with the watermark data. Additionally, the underlying black-box watermark may not set the same label for all the watermark data. In other words, the target label  $y_{wi}$  in watermark data  $X_w$  may be non-fixed and could be

any integer in the set  $\{0, 1, \dots, C-1\}$ . Therefore, we repeat the optimization step in Equation 1 for all possible classes and finally obtain  $C$  batches of recovered samples  $\{B_c\}_{c=0}^{C-1}$ , where  $B_c$  indicates the inverted batch of samples towards class  $c$ . In our design, these samples are expected to contain enough watermark information of  $f_w$ .

Note that although the BN layers keep the statistics of the total training set, including samples of all classes, our watermark recovering method is actually using an aggressive class-wise inversion scheme. This is because our goal is to *recover samples close to the watermark data as much as possible here, instead of to generate realistic images*. Since the watermark data may constitute a large contribution to the BN statistics during the training, we propose this scheme to greedily absorb information in BN layers, preventing it to diffuse into other classes. This design is especially effective against watermarks with fixed target classes, compared to the arbitrary-class scheme in conventional inversion methods [54]. We validate this point in Section 6.4.2.

## 4.2 Watermark Unlearning

Now that we have recovered a set of samples  $\{B_c\}_{c=0}^{C-1}$  containing sufficient watermark information in the target model  $f_w$ , we can deliberately unlearn them during the finetuning process. Directly unlearning these recovered samples without other constraints may cause catastrophic forgetting, bringing irreversible significant damage to its normal performance. In the current framework, we consider two data settings for  $\mathcal{A}$ ’s auxiliary data  $X_{aux}$ , in-distribution and transfer, as defined in Section 3.2. This basic framework is extended to the data-free setting with more improved designs in Section 5.

Assuming the attacker  $\mathcal{A}$  has some in-distribution data

$X_{aux} = \{(x_i, y_i)\}$  from  $f_w$ 's main task, he/she can leverage these labeled samples to preserve model's performance during unlearning. When  $\mathcal{A}$  only has some unlabeled data  $\{x_i\}$  from a different distribution, similar goals can be achieved by leveraging model  $f_w$  as an oracle to generate pseudo-labels for each sample, yielding the transfer dataset  $X_{aux} = \{(x_i, f_w(x_i))\}$ .

Starting from  $f_w$ , the attacker can finetune the surrogate model  $f_a$  under the following optimization objective:

$$\begin{aligned} \min_{\theta_a} & \underbrace{\sum_{(x_i, y_i) \in X_{aux}} \mathcal{L}(f_a(x_i), y_i)}_{\text{preserving original performance}} \\ & + \underbrace{\alpha_{KL} \sum_{B_c \in \{B_c\}_{c=0}^{C-1}} \sum_{\hat{x}_i \in B_c} KL(f_a(\hat{x}_i), y_{soft})}_{\text{removing watermark}}, \end{aligned} \quad (4)$$

where  $\theta_a$  indicates the parameters of  $f_a$ ,  $KL(\cdot)$  is the Kullback–Leibler divergence,  $y_{soft}$  is a soft unlearning target of length  $C$ , where each element equal to  $1/C$ . Note that we are using a more consistent unlearning target, compared to the hard random labels, which might lead to gradient conflicts and cancellations during the fine-tuning process.

The first term in Equation 4 stabilizes the general prediction behavior of  $f_a$  and thus preserves its performance, while the second term encourages  $f_a$  to unlearn the watermark-related information. In this way, we successfully derive a surrogate model  $f_a$  to prevent successful watermark verification.

## 5 Improved Designs for MIRA

In this section, we enhance the general framework of MIRA in the following directions.

1. **Improved Recovering via Target Class Detection:** First, existing black-box watermarks consist of those with fixed target classes and with non-fixed target classes. For watermarks with fixed target classes (such as *Content* [56] and *EWE* [25]), recovering and unlearning watermark data from other classes bring no benefit to watermark removal, and can even sacrifice the utility of the surrogate model. Therefore, after the original watermark recovering stage, we further distinguish whether the underlying watermark has a fixed target class, and detect its target class if so. We only retain recovered samples belonging to the target class for a fixed-class watermark (§5.1).
2. **Improved Unlearning via Recovered Sample Splitting:** Second, the inverted samples derived by Equation 1 may also contain important information of the main task. Indiscriminately unlearning all the inverted samples from the target classes might also hurt the model utility. Therefore, before the original watermark unlearning stage, we split out samples closer to the real watermark data from the recovered ones and improve the finetuning loss accordingly (§5.2).

Our two improved designs, as well as the complete attack workflow, are shown in Fig. 1. Note that the two improvements mainly exploit the properties of the recovered samples obtained from Equation 1 instead of the in-distribution or the transfer auxiliary data, enabling our attack to be extended to a data-free setting for watermarks which are detected to have a fixed target class.

### 5.1 Target Class Detection

• **Insight: Watermark Smoothness.** By inspecting the model watermarking implementations (detailed in §3.1), we find that for a DNN watermark with a fixed target class, the model tends to learn much more diverse data related to the target class during the training, compared to other labels, as, besides normal samples belonging to the target label, all watermark samples are also labeled with the target class. The model also learns samples belonging to the target label more prominently, because of the higher participation ratio of these watermark data for the watermark robustness consideration.

Based on the above observations, we conjecture that, for an over-parameterized model embedded with a fixed-class watermark, the loss landscape (i.e., the structure of loss values around the parameter space of a DNN) is smoother with respect to samples of the target label compared to those of other labels. We call this hypothesis *watermark smoothness*, and will conduct a pilot study to validate it.

• **A Pilot Study.** To validate the watermark smoothness hypothesis, we implement both fixed-class and non-fixed-class black-box watermarks and evaluate the watermarked models' smoothness on all the labels.

A smooth loss landscape can be usually characterized by the robustness of the model to both input-level and parameter-level perturbations [13, 17, 45]. To quantify this smoothness property, we define a metric called *SmoothAcc*. Given a set of samples  $X$ , we calculate the average prediction accuracy of  $(x_i, y_i) \in X$  under perturbations:

$$\text{SmoothAcc}(X) = \frac{1}{|X|} \sum_{(x_i, y_i) \in X} \mathbb{P}(\arg\max_j f_w(x_i + \varepsilon_1; \theta_w + \varepsilon_2)_j = y_i), \quad (5)$$

where  $\varepsilon_1 \in \mathcal{N}(0, \sigma_1^2 I_1)$  is the input-level Gaussian noise and  $\varepsilon_2 \in \mathcal{N}(0, \sigma_2^2 I_2)$  is the parameter-level Gaussian noise.

We inspect ten watermarked ResNet-18 [21] models on CIFAR-10 [28] dataset, embedded with five fixed-class watermarks (with the target class set to 6) and five non-fixed-class watermarks respectively (more details are described in Section 6.1). For each model, we collect 11 batches of samples, including ten batches from normal samples of each class, and one batch from watermark samples, each with a batch size of 100. During smoothness analysis, we set the standard deviations of the Gaussian noise  $\varepsilon_1 = 0.5$  and  $\varepsilon_2 = 0.015$ , and

repeatedly sample the Gaussian noise 100 times for each sample to approximate the possibility  $\mathbb{P}(\cdot)$  in Equation 5. The results are shown in Fig. 2.

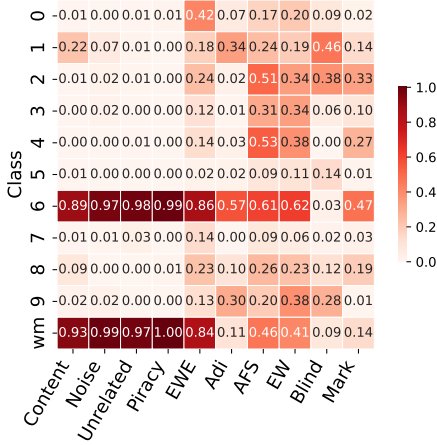


Figure 2: Class-wise smoothness analysis of the ten investigated black-box watermarks on CIFAR-10, via robustness to input-level and parameter-level perturbations. The left five are fixed-class watermarks, while the right five are non-fixed-class watermarks.

Obviously, for fixed-class watermarks, models exhibit much higher smoothness on samples from the target class, including normal and watermark samples, compared to those from other classes. This class-wise smoothness difference is less evident for non-fixed-class watermarks, where models can achieve moderate smoothness on several classes simultaneously.

In summary, the experimental results support the watermark smoothness hypothesis. For a watermarked DNN model embedded with a fixed-class watermark, the loss landscape is expected to be smoother on the target label compared to other labels. In other words, the model is expected to be more robust against input-level and parameter-level perturbations on samples belonging to the target class, including normal samples and watermark samples, compared to those belonging to other classes.

• **Technical Designs.** Based on the observations above, we assume that the watermark smoothness phenomenon also exists, when the target model  $f_w$  is embedded with a fixed-class watermark, in the class-wise inverted samples  $\{B_c\}_{c=0}^{C-1}$ . Supposing the fixed target label is  $y_w$ , then the class-wise smoothness difference would also be significant in  $\{B_c\}_{c=0}^{C-1}$  as the inverted batch  $B_{y_w}$  from the target label will cover the space of both normal samples of  $y_w$  and watermark samples.

In light of this, we propose to evaluate the smoothness of  $f_w$  on  $\{B_c\}_{c=0}^{C-1}$  after the watermark recovering, i.e., to calculate  $\text{SmoothAcc}(B_c)$  for  $c \in \{0, 1, \dots, C-1\}$  respectively. Each  $\hat{x}_i \in B_c$  is temporarily labeled as class  $c$  during the smoothness evaluation. Next, we sort the batches  $\{B_c\}_{c=0}^{C-1}$  according to their  $\text{SmoothAcc}(B_c)$  values in the descending order, yielding sorted  $\{B_{s_0}, B_{s_1}, \dots, B_{s_{C-1}}\}$ . We detect whether  $f_w$  is

embedded with a fixed-class watermark, and, if so, follow the criterion below to determine the target class:

- If the gap between the recovered two batches evaluated with the highest smoothness, i.e.,  $\text{SmoothAcc}(B_{s_0}) - \text{SmoothAcc}(B_{s_1})$ , is larger than a certain threshold  $T$ , we regard the underlying watermark as a fixed-class watermark, and take the target label as  $s_0$ . We then only retain recovered samples  $B_{s_0}$  and drop other batches.
- Otherwise, we regard the underlying watermark as a non-fixed-class watermark, and keep all the recovered batches  $\{B_c\}_{c=0}^{C-1}$  since each class  $c$  might have several correlated watermark samples. We additionally record labels of the last two batches,  $s_{C-1}$  and  $s_{C-2}$ , as the least-likely label and second-least-likely label respectively.

In the remainder of this paper, we use  $\{B_c\}_*$  to denote  $\{B_{s_0}\}$  if a fixed-class watermark is detected, and  $\{B_c\}_{c=0}^{C-1}$  otherwise. Consequently, after the watermark recovering and target label detection, we get batch(es) samples  $\{B_c\}_*$  which are close to real watermark data  $X_w$ .

## 5.2 Recovered Samples Splitting

• **Insight: Normal Data Dominance.** Meanwhile, we derive another observation called *normal data dominance* that, for a watermarked model (either with fixed or non-fixed target classes), *the normal data tend to occupy a larger space than the watermark data in the model's decision region*. Generally, existing black-box watermark schemes involve the normal data in dominance during training for reducing the utility loss [3, 7]. Meanwhile, the watermark samples in minority are usually different from the main task's distribution. Given a much higher training involvement, the model tends to quickly fit the watermark data at the very beginning (a similar phenomenon is found in the backdoor literature [35]). On the contrary, normal samples of the main task are more similar, which provide more abundant and sustained gradient updates throughout the training. Therefore, we conjecture that for each class  $c$  of a watermarked model  $f_w$ , the watermark samples those labeled as  $c$ , if present, are expected to occupy a smaller space than the normal samples in the decision region of the  $c$ -th class.

• **A Pilot Study.** It is challenging to directly compare the occupied space of normal and watermark samples in each class's decision region, due to the difficulty of depicting the abstract decision region itself. To address this issue, we take a slightly different approach and examine the recovered samples from each class, which provides a feasible approximation to the current class's decision region. Moreover, we tactfully distinguish the space occupied by normal and watermark samples via analysis on their *exclusive salient neurons*.

To formally depict the saliency of neurons, we use an existing metric called *importance score* [11]. Specifically, given a batch of samples  $X_c$  belonging to the same class  $c$ , we cap-

Table 3: Normal data dominance analysis of DNNs protected by ten black-box watermarks on class 6, CIFAR-10.

| Neuron Type                     | Content | Noise | Unrelated | Piracy | EWE  |
|---------------------------------|---------|-------|-----------|--------|------|
| $ESN(X_{nor}), ESN(X_{wmk})$    | 335     | 340   | 322       | 380    | 290  |
| $SN(X_{inv}) \cap ESN(X_{nor})$ | 159     | 147   | 207       | 261    | 149  |
| $SN(X_{inv}) \cap ESN(X_{wmk})$ | 22      | 26    | 12        | 0      | 60   |
| Neuron Type                     | Adi     | AFS   | EW        | Blind  | Mark |
| $ESN(X_{nor}), ESN(X_{wmk})$    | 219     | 198   | 211       | 231    | 266  |
| $SN(X_{inv}) \cap ESN(X_{nor})$ | 112     | 101   | 112       | 132    | 112  |
| $SN(X_{inv}) \cap ESN(X_{wmk})$ | 67      | 63    | 45        | 71     | 68   |

ture the activation values of neurons at the  $l$ -th layer, i.e.,  $f_{w(l)}(X_c)$ , and calculate an importance score for each  $j$ -th neuron:  $Imp_t(f_{w(l)}(X_c)_j) = \frac{\mu_j}{\sigma_j}$ , where  $\mu_j$  and  $\sigma_j$  are the mean and the standard deviation of the  $j$ -th neuron estimated on  $X_c$ . Intuitively, a high importance score implies a significant and stable neuron for  $X_c$ . We refer to the neurons with top-5% importance score as salient neurons for  $X_c$  (denoted as  $SN(\cdot)$ ). As normal samples and watermark samples tend to rely on different salient neurons [11, 25, 37], we define the exclusive salient neurons as the subset of salient neurons that are exclusive to each type (denoted as  $ESN(\cdot)$ ).

With this tool, we investigate ten watermarked models embedded with five fixed-class (with target label 6) and five non-fixed-class watermarks in Table 1. Given the inverted samples  $X_{inv}$  from the target class, clean samples from the target class of the training set  $X_{nor}$ , and all the ground-truth watermark samples of class 6, i.e.,  $X_{wmk}$ . As is shown in Table 3, both the fixed-class and non-fixed-class watermarks witness a larger occupied space for the normal data. For example,  $SN(X_{inv})$  intersects more with  $ESN(X_{nor})$ , compared to with  $ESN(X_{wmk})$ . For non-fixed-class watermarks, the normal data dominance observation still holds, but is slightly less evident compared to fixed-class watermarks, possibly due to their more complex input-output pairing relation, which leaves the watermark data more entangled with normal data when the model contains non-fixed-class watermarks. Note that this does not conflict with the goal of the watermark recovering stage. In fact, samples close to the real watermark data still exists in the inverted batch (even for the *Piracy* watermark in Table 3), but less evident in a batch-wise statistical view, compared to those close to the normal data.

• **Technical Designs.** As the class-wise inverted samples might also contain important information of the normal samples, here we attempt to identify those closer to real watermark data in each inverted batch samples  $B_c$  by analysing the salient neurons. Based on the observation of normal data dominance, most of the information in the inverted samples should be relevant to the normal samples. Hence, for each class  $c$ , the salient neurons of its normal samples can be approximately represented by the salient neurons of the total inverted batch  $B_c$ . As the normal samples and watermark samples tend to rely on different salient neurons [11, 25, 37], we can consider the subset of  $B_c$  which are least frequently activated on the

salient neurons of  $B_c$  to be more relevant to the watermark task. Algorithm 1 in Appendix A.2 lists the detailed splitting procedure.

Given the recovered samples  $\{B_c\}_*$  obtained via watermark recovering and target label detection, the algorithm will perform class-wise splitting on each batch  $B_c$ , and return samples closer to the watermark data, namely proxy watermark data  $\{B_{c,wmk}\}_*$ , leaving the rest in each batch as closer to the normal data, namely proxy normal data  $\{B_{c,nor}\}_*$ . Finally, we improve the finetuning loss accordingly. If the target model is detected with a fixed-class watermark (i.e., the target class  $s_0$ ), we only need to unlearn samples from class  $s_0$ , denoted as  $\{B_{c,wmk}\}_* = \{B_{s_0,wmk}\}$  and  $\{B_{c,nor}\}_* = \{B_{s_0,nor}\}$ . In this way, the attacker can finetune the surrogate model  $f_a$  under the following objective:

$$\min_{\theta_a} \underbrace{\left( \sum_{(x_i, y_i) \in X_{aux}} \mathcal{L}(f_a(x_i), y_i) \right)}_{\text{preserving original performance}} + \underbrace{\sum_{\hat{x}_i \in B_{s_0, nor}} \mathcal{L}(f_a(\hat{x}_i), s_0)}_{\text{removing watermark}} \quad (6)$$

$$+ \underbrace{\sum_{\hat{x}_i \in B_{s_0, wmk}} \mathcal{L}(f_a(\hat{x}_i), \text{rand}_{s_0})}_{\text{removing watermark}},$$

where  $\text{rand}_{s_0}$  denotes a random label in  $\{0, 1, \dots, C-1\}$  except  $s_0$  itself. This unlearning target is stronger than that in Equation 4, due to the enhanced specificity brought by target label detection. Note that in the objective function above, we additionally exploit the proxy normal data  $B_{s_0, nor}$  to preserve  $f_a$ 's original performance. This design enables our MIRA to be extended to a data-free setting: when the auxiliary data is not available (i.e., the first term enclosed by  $(\cdot)$  in the above equation is optional), we can still perform watermark unlearning only using the recovered samples.

For non-fixed-class watermarks,  $\{B_{c,wmk}\}_*$  contains  $C$  batches of proxy watermark data. Then  $\mathcal{A}$  can finetune  $f_a$  under this objective:

$$\min_{\theta_a} \underbrace{\sum_{(x_i, y_i) \in X_{aux}} \mathcal{L}(f_a(x_i), y_i)}_{\text{preserving original performance}} + \underbrace{\sum_{B_{c, wmk} \in \{B_{c, wmk}\}_*} \sum_{\hat{x}_i \in B_{c, wmk}} \mathcal{L}(f_a(\hat{x}_i), y_*)}_{\text{removing watermark}}, \quad (7)$$

where  $y_*$  denotes the least-likely label  $s_{C-1}$  (obtained during the target class detection process) for  $B_{c, wmk} \in \{B_{c, wmk}\}_*$  and  $c \neq s_{C-1}$ , while the second-least-likely label  $s_{C-2}$  when  $c = s_{C-1}$ . This proxy label unlearning target is also stronger than that in Equation 4. Different from the design for fixed-class watermarks, we do not use proxy normal data to further preserve the model performance. This is because the normal data dominance phenomenon is less evident for non-fixed-class watermarks (Table 3), and thus the salient neurons of



the split proxy normal data might still have some intersection with those of the real watermark data. Therefore, leveraging these proxy normal data for preserving utility might hinder the watermark removal.

## 6 Experiments

### 6.1 Overview of Evaluation

To evaluate the removal effectiveness of MIRA, we perform a comprehensive study on the vulnerability of ten state-of-the-art black-box watermarking schemes listed in Table 1. Before presenting the detailed evaluation results, we first provide a concise introduction to the experimental setups.

- **Datasets and Victim Models.** Following the settings in [25, 33, 43], we construct victim models on three benchmark datasets, namely, MNIST [31], CIFAR-10 and CIFAR-100 [28]. The respective DNN architectures are LeNet-5 [30], ResNet-18 [21] and ResNet-34. We embed black-box watermarks into the victim models during the training. Then we perform watermark removal attacks including MIRA and the baseline attacks to evaluate their effectiveness.

- **Target Watermark Schemes.** Our evaluation covers ten existing black-box DNN watermarks, which are categorized as *fixed-class watermarks* (i.e., all the watermark data are paired with the identical target class), and *non-fixed-class watermarks* (i.e., each watermark data is paired with its own target class) listed in Table 1. For more backgrounds on the watermarking schemes, please refer to Appendix B.1. We implement the target black-box watermark schemes based on the open-source watermark framework provided by Lederer et al. [32], with target class set to 6 for the fixed-class watermarks. For the watermarks not included in the framework (such as EWE and Blind), we strictly follow the parameter settings described in the original papers. For more implementation details and the performance of the watermarked models, please refer to Appendix B.2 and B.3.

- **Baseline Removal Attacks.** We compare our MIRA with the following three types of removal attacks, six baseline attacks in total.

- *Pruning-based attacks:* (1) **Pruning** [48, 56] directly sets a proportion of DNN parameters with the smallest absolute values to zero. (2) **Fine-pruning** [37] prunes neurons that are infrequently activated by normal data, followed by a finetuning process.
- *Finetuning-based attacks:* (3) **Finetuning** [8, 9] specifically finetunes the target model using a large learning rate, together with a carefully-designed scheduler. (4) **Regularization** [39, 43] finetunes the target model with a large L2 regularization on the parameters. (5) **Distraction** [58] finetunes the target model on in-distribution or transfer data, together with another set of lure data that distracts the model’s attention away from the watermark.

- *Unlearning-based attacks:* (6) **Laundering** [4] leverages trigger reverse-engineering methods [50] in backdoor defense literature to recover watermark data, followed by neuron resetting and model retraining, to remove backdoor-based watermarks.

The implementation details of these baseline attacks are clarified in Appendix B.4.

- **Implementation of MIRA.** During watermark recovering, we set hyper-parameters  $M = 250, \alpha_{\ell_2} = 0.01, \alpha_{\ell_v} = 0.03, \alpha_{bn} = 0.1$ . We use  $\tanh(\cdot)$  to constrain the batch data within a valid range, and optimize the recovering objective with the Adam optimizer of learning rate 0.1. For target label detection, we set  $\sigma_1 = 1.0, \sigma_2 = 0.03$  for MNIST and  $\sigma_1 = 0.5, \sigma_2 = 0.015$  for CIFAR-10 and CIFAR-100 respectively. The detection threshold  $T$  is conservatively set to 0.4 for MNIST and CIFAR-10, while 0.3 for CIFAR-100. For splitting the recovered samples, we set  $l$  to be the penultimate layer of the target model, and saliency ratio  $\beta = 0.95$ , split ratio  $\gamma = 0.5$  in Alg. 1. During watermark unlearning, we set  $\alpha_{KL} = 15$  to ensure the unlearning strength for the basic MIRA and the uniform loss weights for the improved MIRA. The model is finally finetuned for 10 epochs using the SGD optimizer with the batch size 128. The learning rate is set to 0.01 when auxiliary data is available and 0.003 when data-free. Noteworthily, the settings above are empirically chosen and lead to strong attack effectiveness uniformly over almost all the covered watermarking schemes, which supports the watermark-agnostic nature of our MIRA.

- **Evaluation Metrics.** We primarily focus on the utility and the watermark retention of the surrogate models obtained via removal attacks. Specifically, we use *clean accuracy*, i.e., the classification accuracy on the test set, to measure the utility, and *watermark accuracy*, i.e., the ratio of watermark samples correctly classified as target labels, to measure the watermark retention. To compare the attack effectiveness over different black-box watermark schemes, we follow Lukas et al. [39] to determine the decision threshold  $\theta$  for each watermark on 20 independently trained clean models, and then calculate a metric called the *rescaled watermark accuracy*. The linear rescaling function is defined as  $S(x; \theta) = \max(0, \frac{1-\theta'}{1-\theta}x + \frac{\theta'-\theta}{1-\theta})$ , which degrades to  $S(x; \theta) = \max(0, 1 - 0.5 \frac{1-x}{1-\theta})$  when we set  $\theta' = 0.5$ . Rescaled watermark accuracy unifies the watermark accuracy of surrogate models embedded with different watermarks. According to [39], the model watermark is fully removed if the rescaled watermark accuracy is lower than 50%. Table B.1 in Appendix B.3 summarizes our estimated decision threshold for the ten black-box watermarking schemes.

We define a removal attack is successful (i.e., cracks the target watermark scheme) if the rescaled watermark accuracy is below 50% and the surrogate model maintains at least 90% of the original utility. Note that our attack success criterion is slightly different from [39] in that they consider a maximum

Table 4: Comparison of removal attacks against black-box DNN watermarks under the in-distribution setting on CIFAR-10.  $x / y$  denotes the clean accuracy / rescaled watermark accuracy, and values behind  $\pm$  report their standard deviations respectively in 5 repetitive tests. The rescaled watermark accuracy values below 50% are bolded and underlined. The left five columns are attack results of the fixed-class watermarks, while the right five are of the non-fixed-class watermarks.

| Attacks               | Content                   | Noise                    | Unrelated                 | Piracy                    | EWE                       | Adi                       | AFS                       | EW                        | Blind                     | Mark                      |
|-----------------------|---------------------------|--------------------------|---------------------------|---------------------------|---------------------------|---------------------------|---------------------------|---------------------------|---------------------------|---------------------------|
| None                  | 93.8 / 100.0              | 94.1 / 100.0             | 93.7 / 100.0              | 93.3 / 100.0              | 94.0 / 100.0              | 93.9 / 100.0              | 93.0 / 100.0              | 92.9 / 100.0              | 91.2 / 100.0              | 94.0 / 100.0              |
| <i>Fine-pruning</i>   | 86.4 / <b><u>44.7</u></b> | 87.4 / 67.0              | 85.9 / 52.6               | 69.5 / <b><u>37.8</u></b> | 88.9 / 70.2               | 85.4 / 59.8               | 87.3 / 80.4               | 87.6 / 83.3               | 77.0 / 53.8               | 87.3 / 61.1               |
| <i>Finetuning</i>     | 85.5 / <b><u>46.4</u></b> | 85.1 / 84.9              | 84.6 / <b><u>47.1</u></b> | 66.1 / <b><u>40.9</u></b> | 86.9 / 81.2               | 85.0 / 56.3               | 90.4 / 99.4               | 90.1 / 98.8               | 79.9 / 55.0               | 85.8 / 57.1               |
| <i>Regularization</i> | 60.3 / 100.0              | 54.7 / 91.5              | 82.8 / 100.0              | 76.9 / 100.0              | 68.2 / <b><u>47.6</u></b> | 55.4 / 73.8               | 72.3 / 81.6               | 69.0 / 82.1               | 69.8 / 83.6               | 75.7 / 87.2               |
| <i>Distraction</i>    | 87.4 / <b><u>47.5</u></b> | 89.5 / 98.1              | 88.5 / 51.5               | 70.6 / <b><u>40.9</u></b> | 85.8 / 52.4               | 89.4 / 52.2               | 92.5 / 99.4               | 92.5 / 100.0              | 89.8 / 91.2               | 86.0 / 51.3               |
| <i>Laundering</i>     | 91.1 / <b><u>48.1</u></b> | 90.7 / 77.4              | 88.8 / 100.0              | 83.8 / 69.9               | 91.1 / 70.2               | 87.0 / 69.7               | 89.3 / 100.0              | 89.3 / 98.8               | 86.3 / 73.1               | 91.1 / 94.8               |
| MIRA (Basic)          | 88.8 / <b><u>44.7</u></b> | 88.1 / <b><u>5.7</u></b> | 88.1 / <b><u>44.9</u></b> | 83.3 / <b><u>44.0</u></b> | 89.0 / <b><u>48.2</u></b> | 84.1 / 51.6               | 86.4 / <b><u>44.9</u></b> | 85.2 / 52.1               | 84.1 / 58.5               | 83.0 / 50.7               |
| MIRA (Improved)       | 93.1 / <b><u>45.8</u></b> | 93.1 / <b><u>5.7</u></b> | 92.7 / <b><u>44.9</u></b> | 91.4 / <b><u>41.5</u></b> | 93.3 / <b><u>47.6</u></b> | 86.0 / <b><u>49.3</u></b> | 88.1 / <b><u>44.3</u></b> | 88.2 / <b><u>46.3</u></b> | 90.1 / <b><u>46.2</u></b> | 88.5 / <b><u>47.2</u></b> |

5% utility loss. This is mainly because we consider the more realistic data-limited settings (e.g., 2% of the source training set in Section 6.2), while they assume the attacker has access to over 30% of the training set.

## 6.2 Attack Performance

We evaluate the performance of removal attacks in each scenario in Section 3.2, namely, in-distribution, transfer and data-free settings. The comparison with baseline removal attacks is organized according to the data settings where the baseline attacks are applicable. Due to the page limit, we mainly present and analyze the attack results on CIFAR-10, while similar results are observed on MNIST and CIFAR-100. Appendix C.1 and C.2 present the omitted results.

**(1) In-distribution Setting.** We first evaluate the attack performance of our MIRA under the in-distribution data setting. Following [58], the attacker is assumed to have 1000 normal samples from the source training set (i.e. 2% of the CIFAR-10 training set). Table 4 presents the clean accuracy and the rescaled watermark accuracy of the surrogate models, after performing different removal attacks on the victim model protected by one of the ten black-box watermarks.

**Results & Analysis.** As Table 4 shows, both the basic MIRA and improved MIRA significantly lower the rescaled watermark accuracy of surrogate models, among which the improved MIRA achieves comprehensive watermark removal against the ten investigated black-box watermarks, with at least 90% utility preserved (six in ten even with a clean accuracy degradation in 2%).

The baseline removal attacks are only effective against a subset of watermark schemes. For instance, *Laundering* is more effective against watermarks similar to backdoors, such as *Content*, *Piracy* and *EWE*, but less effective against other watermarks, because of its dependence on the trigger reverse-engineering method to detect and remove the underlying watermarks. *Fine-pruning* and *Finetuning* are less effective against *EWE*, *Adi* and *AFS*, possibly due to the more entangled learned representations of the watermark data. *Distraction* can also only compromise about half of these watermarks’ robustness, while being less powerful against watermarks of other

forms. In contrast, our basic and improved MIRA are both effective regardless of the target watermark schemes, due to the capture of the black-box watermarks’ commonality. Note that our improved MIRA can effectively remove the *Piracy* watermark, despite the fact that the number of its watermark data (1% of the training data, i.e., 500, following the original paper) is much larger than the number of unlearned samples in our improved MIRA ( $\gamma \times M = 125$ ). This indicates that the removal effect of our approach is achieved not just through a sample-level coverage, but also through a deeper level of neuron coverage.

Additionally, these baseline attacks might impact the surrogate model’s utility seriously. For instance, the finetuning-based attacks, such as *Finetuning*, *Regularization* and *Distraction*, incur a large clean accuracy degradation against *Noise* and *Piracy* watermarks, possibly due to their overly offensive finetuning strategies. However, our MIRA attacks could still preserve the surrogate model’s performance besides removing the watermark, because of their more specific training (unlearning) objectives.

We further compare the attack results of our basic MIRA and improved MIRA separately in Fig.3. Obviously, the improved MIRA preserves more clean accuracy than the basic MIRA against all watermarks, with a 4% increase in average, due to the enhanced removal specificity brought by target class detection and recovered samples splitting algorithms. Noteworthy, the improved MIRA is even stronger than the basic MIRA, which could be explained by the simpler and directer unlearning objective.

**(2) Transfer Setting.** Next, we evaluate the attack performance under the transfer data setting. Here the attacker cannot access the source training data, but is assumed to have 2000 unlabeled samples from another distribution (e.g., CIFAR-100 for target models trained on CIFAR-10, following [19, 58]). Table 5 presents the attack results under this setting.

**Results & Analysis.** As we can see from Table 5, the clean accuracy of the surrogate models are generally lower than those under the in-distribution setting, since the proxy labels of these transfer data may contain noise. Regularization is generally less effective, and *Distraction* is only effective against a subset of fixed-class watermarks.

Table 5: Comparison of removal attacks against black-box watermarks under the transfer setting on CIFAR-10.

| Attacks         | Content            | Noise             | Unrelated          | Piracy             | EWE                | Adi          | AFS                | EW                 | Blind              | Mark               |
|-----------------|--------------------|-------------------|--------------------|--------------------|--------------------|--------------|--------------------|--------------------|--------------------|--------------------|
| None            | 93.8 / 100.0       | 94.1 / 100.0      | 93.7 / 100.0       | 93.3 / 100.0       | 94.0 / 100.0       | 93.9 / 100.0 | 93.0 / 100.0       | 92.9 / 100.0       | 91.2 / 100.0       | 94.0 / 100.0       |
| Regularization  | 49.3 / 99.4        | 60.3 / 73.6       | 53.1 / 100.0       | 60.5 / 100.0       | 53.8 / <b>47.6</b> | 41.0 / 69.7  | 43.4 / 71.5        | 55.5 / 76.9        | 44.6 / 69.6        | 53.4 / 74.5        |
| Distraction     | 89.0 / 50.9        | 89.6 / 100.0      | 88.7 / <b>49.8</b> | 84.2 / <b>49.0</b> | 88.8 / 63.4        | 87.7 / 60.3  | 92.0 / 100.0       | 92.3 / 100.0       | 88.8 / 91.2        | 89.1 / 66.9        |
| MIRA (Basic)    | 85.5 / <b>49.8</b> | 85.3 / <b>6.7</b> | 80.0 / <b>46.0</b> | 82.4 / <b>45.2</b> | 88.2 / 50.8        | 80.8 / 54.5  | 84.6 / <b>48.1</b> | 82.1 / 58.5        | 80.2 / 62.0        | 84.0 / 55.9        |
| MIRA (Improved) | 92.5 / <b>47.0</b> | 92.3 / <b>5.7</b> | 92.7 / <b>48.2</b> | 90.1 / <b>47.1</b> | 92.6 / <b>49.7</b> | 80.4 / 59.8  | 86.2 / <b>47.4</b> | 83.5 / <b>49.8</b> | 88.8 / <b>46.8</b> | 87.0 / <b>49.5</b> |

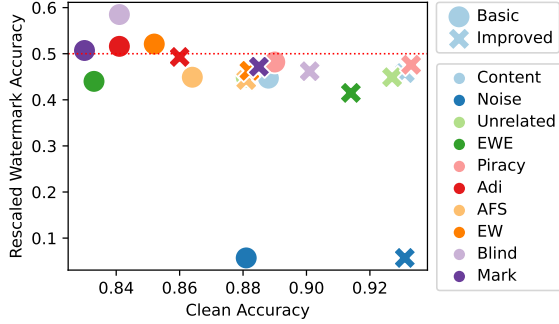


Figure 3: Comparison of the basic and the improved MIRA under the in-distribution setting on CIFAR-10.

Table 6: Comparison of removal attacks against black-box watermarks under the data-free setting on CIFAR-10.

| Attacks         | Content            | Noise              | Unrelated          | Piracy             | EWE                |
|-----------------|--------------------|--------------------|--------------------|--------------------|--------------------|
| None            | 93.8 / 100.0       | 94.1 / 100.0       | 93.7 / 100.0       | 93.3 / 100.0       | 94.0 / 100.0       |
| Pruning         | 81.5 / 78.2        | 90.7 / <b>42.5</b> | 78.7 / <b>45.4</b> | 41.9 / <b>37.8</b> | 92.2 / 100.0       |
| MIRA (Improved) | 89.8 / <b>45.8</b> | 88.6 / <b>5.7</b>  | 88.8 / <b>46.0</b> | 90.0 / <b>39.6</b> | 90.7 / <b>48.2</b> |

On the contrary, both the basic and improved MIRA significantly lower the rescaled watermark accuracy while preserving the clean accuracy at an acceptable level. The improved MIRA still successfully cracks nine of the ten watermarks under this setting. Note that our MIRA cannot completely remove the *Adi* watermark (despite the rescaled watermark accuracy is lower than 60%) under the transfer setting. This is reasonable because *Adi* uses abstract out-of-distribution images as watermark data, whose salient neurons are more likely to be activated by the transfer dataset, compared to other common watermarks.

**(3) Data-free Setting.** Moreover, we evaluate the effectiveness of MIRA under the data-free setting, which means the attacker cannot access any samples. Almost no baseline attacks except for the Pruning attack are applicable to the data-free scenario. Therefore, as also explained in Section 5.2, we mainly compare the improved MIRA, when attacking five fixed-class watermarks here, with Pruning. The attack results are shown in Table 6.

**Results & Analysis.** As Table 6 shows, our improved MIRA achieves surprisingly good performance in the data-free setting, and significantly surpasses the baseline Pruning. All the five fixed-class watermarks are completely removed from the protected model, with a clean accuracy degradation of no more than 5.5%. This validates the correctness of our splitting algorithm on the recovered samples, since the sur-

Table 7: Attack results of improved MIRA on CIFAR-10 and CIFAR-100, with the target class detection results deliberately set to fixed-class and non-fixed-class ones, respectively.

| Dataset   | Detection | Content            | Piracy             | Adi                | AFS                |
|-----------|-----------|--------------------|--------------------|--------------------|--------------------|
| CIFAR-10  | fixed     | 93.1 / <b>45.8</b> | 91.4 / <b>41.5</b> | 92.0 / 96.5        | 88.8 / 93.7        |
|           | non-fixed | 90.7 / <b>44.2</b> | 88.9 / <b>40.3</b> | 86.0 / <b>49.3</b> | 88.1 / <b>44.3</b> |
| CIFAR-100 | fixed     | 75.1 / <b>48.7</b> | 71.0 / <b>41.8</b> | 64.0 / 71.5        | 67.1 / 100.0       |
|           | non-fixed | 67.7 / <b>48.7</b> | 65.8 / <b>40.0</b> | 64.8 / 60.3        | 65.4 / 54.8        |

rogate modes are finetuned solely on the recovered samples  $\{B_c\}_* = \{B_{s_0}\}$ , with split proxy normal data  $\{B_{s_0,nor}\}$  to maintain the utility, and proxy watermark data  $\{B_{s_0,wmk}\}$  to remove watermarks, as in Equation 6.

### 6.3 Validating Detection of Target Classes

In this part, we mainly study the risks of target class detection errors. We temporarily ignore the case when fixed-class watermarks are correctly identified but given the incorrect target label, since this is extremely rare, as validated by later quantitative experiments. Here we mainly focus on two types of errors, false positives (non-fixed-class watermarks identified as fixed-class ones) and false negatives (fixed-class watermarks identified as non-fixed-class ones). We select two representative fixed-class watermarks, i.e., *Content* and *Piracy*, as well as two non-fixed-class watermarks, i.e., *Adi* and *AFS*, and perform the improved MIRA under the in-distribution data setting. Table 7 presents the unlearning results after identifying the target watermark as fixed-class and non-fixed-class types respectively.

For fixed-class watermarks wrongly identified as non-fixed-class ones, the clean accuracy will degrade a little (e.g., within 3% on CIFAR-10) and the watermark is still effectively removed. However, for non-fixed-class watermarks falsely identified as fixed-class ones, the watermark removal effects will be significantly hampered (e.g, the rescaled watermark accuracy remains over 90%). Compared with false negative, we have a lower tolerance for false positives, and hence we should set the detection threshold conservatively.

Next, we further investigate the detection accuracy of our target class detection algorithm. For each watermark scheme on each dataset, we independently train ten watermarked models, each using the randomly re-generated watermark data with different target classes. For each target watermarked model, we perform watermark recovering and then target class detection. We calculate the SmoothAcc gap  $SmoothAcc(B_{y_w}) - \max_{i \neq y_w} SmoothAcc(B_i)$  for a fixed-

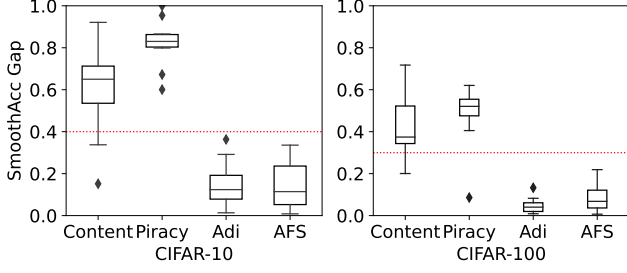


Figure 4: SmoothAcc gap distribution under ten random tests, with randomly re-generated watermark samples and different target classes. Box plot shows min/max and quartiles, as well as the estimated outliers.

class watermark with target class  $y_w$ , and  $\text{SmoothAcc}(B_{s_1}) - \text{SmoothAcc}(B_{s_2})$  for a non-fixed-class watermark. As shown in Fig. 4, the SmoothAcc gaps for fixed-class watermarks are always positive in the ten tests, which means we can always determine a correct target class for those successfully identified fixed-class watermarks. Besides, the SmoothAcc gaps of fixed-class and non-fixed-class watermarks have substantial differences to find a threshold to determine them, which validates the correctness of our target class detection algorithm.

## 6.4 Ablation Studies

### 6.4.1 Understanding Recovering and Unlearning

Furthermore, we conduct an in-depth inspection of our improved MIRA under the data-free setting, to demonstrate its recovering and unlearning mechanism. We focus on the black-box watermark *EWE*, which achieves state-of-the-art robustness in [33]. Fig. 5 visualizes the feature distribution of the target model before and after the attack. Before the attack, the watermark data are well entangled with the normal data of class 6, which follows the design of *EWE*. Our recovered batch data  $B_6$  covers a large portion in class 6’s decision region, with the proxy watermark data  $B_{6,wmk}$  being closer to the real watermark samples, compared with the proxy normal data  $B_{6,nor}$ . This is consistent with our attack design as the splitting design in Section 5.2 tends to find proxy watermark data less intersected with the main distribution, i.e., they are more likely to activate the salient neurons of the real watermark data. After the attack, the general performance of the surrogate model is still preserved, thanks to the proxy normal data  $B_{6,nor}$ . On the other hand, the real watermark data are pushed out of the class 6’s decision region and successfully removed, due to the unlearning process on  $B_{6,wmk}$ .

### 6.4.2 Comparison with Other Recovering Methods

We further prove the effectiveness of the watermark recovering algorithm in MIRA, by comparing with representative algorithms from (1) **Trigger Reverse-Engineering** (e.g., an

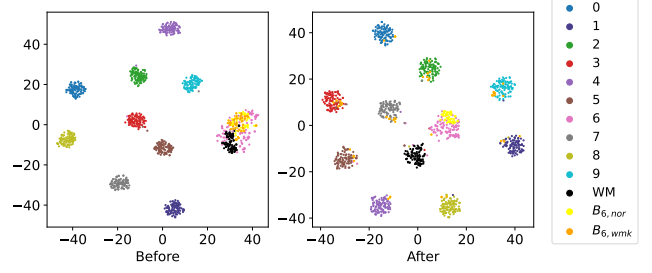


Figure 5: **Visualization of our improved MIRA removing watermark data from their fixed target classes  $y_w = 6$ .** The black, yellow and orange points denote the real watermark data, the proxy normal data  $B_{6,nor}$  and proxy watermark data  $B_{6,wmk}$  split from the inverted batch  $B_6$  from the target class. For visualization, we use TSNE [49] to perform dimensionality reduction on features of data in the penultimate layer of ResNet-18 on CIFAR-10.

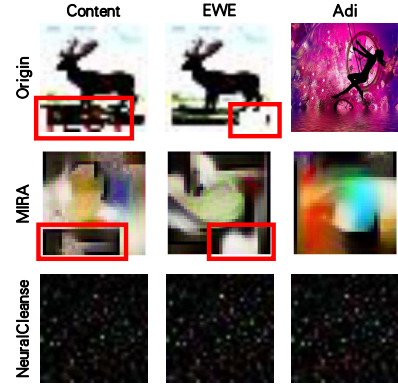


Figure 6: Visualization of recovered watermark images/trigger patterns by MIRA/NeuralCleanse.

adaptive version of *NeuralCleanse* [50]), which is originally designed to detect and erase backdoors in DNNs, and (2) **General Model Inversion** (e.g., DeepInversion [54]), which is designed to synthesizing realistic training samples of the target models for privacy disclosure or knowledge distillation. Our experiments below focus on the in-distribution data setting on CIFAR-10, and perform watermark removal attacks against three black-box watermarks, *Content*, *EWE* and *Adi*.

**Results & Analysis.** Fig. 6 visualizes the recovered watermark data by MIRA and the trigger patterns by *NeuralCleanse*. As is shown, the recovered triggers by *NeuralCleanse* are visually meaningless, and rather similar to each other. This implies that the assumed shortcut in the model’s decision space is non-existent in these watermarked models. The recovered triggers are only the universal adversarial perturbations of the CIFAR-10 dataset itself, irrelevant to the underlying black-box watermarks. In comparison, most of the recovered watermark data holds the essential feature of the watermark pattern specified by the model owner, such as the dark text shapes for *Content*,



Table 8: Attack results using different recovering methods on CIFAR-10.

| <b>Inversion Method</b> | <b>Content</b>     | <b>EWE</b>         | <b>Adi</b>         |
|-------------------------|--------------------|--------------------|--------------------|
| MIRA                    | 92.6 / <b>44.7</b> | 92.5 / <b>48.2</b> | 85.1 / <b>48.7</b> |
| <i>NeuralCleanse</i>    | 92.5 / <b>47.5</b> | 92.2 / 98.4        | 84.4 / 93.0        |
| <i>DeepInversion</i>    | 91.3 / 68.7        | 91.2 / 99.0        | 84.3 / <b>49.3</b> |

and the white patches for EWE. Fig.C.1 in Appendix C.3 also compares the recovered samples of MIRA and DeepInversion.

More quantitatively, we investigate the removal effectiveness using the three recovering methods, with attack results shown in Table 8. As we can see, only the recovered watermark data by our MIRA is effective for removing all the three types of black-box watermarks from the protected models, which further supports the aggressive recovering of MIRA does produce samples informative of the watermark information. For more detailed experimental settings and analysis, please refer to Appendix C.3.

## 7 Discussion

**Black-box DNN Watermarks and Backdoors.** In previous literature, black-box watermarks are sometimes called backdoor-based [4, 38, 43] or trigger set-based watermarks [33]. However, the former has substantial differences from the latter in terms of the watermark data patterns and target class settings (§ 2). First, fixed-class watermarks usually collect samples from a certain source class, add watermark patterns and label them to a fixed target class [25, 56]. In comparison, backdoor attacks apply the trigger to samples from all classes and expect any samples with the trigger to be classified as the target class. Also, these watermark samples from the same source class might be added with different watermark patterns [56], compared to the fixed trigger pattern in traditional backdoors. Non-fixed-class watermarks have even more differences, such that each watermark sample is paired with its own target class, which makes the watermarked model memorize them without learning other backdoor behaviours. Therefore, attacking black-box watermarks has its unique challenges. This also explains why existing removal attacks extended from backdoor defenses, such as *Laundering* (§6.2) and *NeuralCleanse* (§6.4.2), could not effectively remove most of the watermarks.

**Attack Efficiency.** For a target model with a large number of class labels, the main computation cost of MIRA comes from the class-wise watermark recovering process, which is proportional to the number of classes. Similar to the solutions in *NeuralCleanse* [50], we find parallel computation on multiple GPUs and early-stopping mechanisms also useful here. Moreover, we propose a multi-class inversion mechanism during optimizing a single data batch, where the BN regularization term is calculated for samples of each class separately. This modification ensures the class-wise inversion nature and fur-

ther accelerates the recovering process by hosting multiple recovering tasks simultaneously in one GPU.

**Potential Defenses.** In this part, we analyze the potential adaptive defenses against MIRA. First, the owner may try to bypass the target class detection algorithm. For example, when conducting non-fixed-class watermarking, the owner may mislead the target class detection algorithm to produce a false positive result by, e.g., intentionally crafting 300 watermark samples with the specified target class 6 and another 100 watermark samples with random classes. However, in our preliminary studies, this mitigation would cause about 25% utility loss, and the verification success rate of this adaptive watermark after MIRA would still decrease to be lower than 50%. Also, the model owner may attempt to bypass the recovered samples splitting algorithm, by deliberately adding more watermark samples into the target classes and disrupt the dominance of normal data. This would increase the utility loss of the improved MIRA in data-limited settings, while the attacker may skip the splitting procedure and restore the attack effectiveness with in-distribution/transfer data.

**Limitations and Future Works.** First, MIRA leverages the recovering and unlearning to remove the black-box watermarks in DNNs. This ensures its general effectiveness, but might slightly affect the surrogate model’s utility for some non-fixed-class watermarks in our experiments in data-limited settings (e.g., 2% of the training data). Nevertheless, considering the trend of open AI data hubs (e.g., Huggingface Datasets [1]), the attacker is able to find public data from similar domains which can further reduce the utility loss to a desirable level. Second, as existing black-box DNN watermarking schemes cannot be exhausted, we have tried our best to cover most of the black-box watermarking schemes studied in a recent SoK paper [39] as our attack targets. Future works may consider evaluating our attack on more newly proposed black-box schemes before claiming the robustness.

## 8 Conclusion

In this paper, we summarize the commonality of existing black-box DNN watermarks in specially memorizing watermark data correlated to the target labels. Based on this, we uncover a new removal attack surface via recovering and unlearning watermark samples from a target watermarked model. Our novel attack MIRA is watermark-agnostic and effective against most of mainstream black-box DNN watermarking schemes. In addition, we further improve the basic MIRA by target label detection and recovered samples splitting, based on in-depth analysis and observations on the existing black-box watermark schemes. The improved MIRA reduces the utility loss and achieves data-free watermark removal on half of the watermark schemes. Our comprehensive evaluation of MIRA strongly validates its effectiveness in watermark removal, with low utility loss and under more relaxed or even no assumptions on the dataset availability.

## References

- [1] Hugging Face Datasets. <https://huggingface.co/docs/datasets/index>. Accessed: 2023-06-01.
- [2] Protecting intellectual property of deep neural networks with watermarking. <https://research.ibm.com/publications/protecting-intellectual-property-of-deep-neural-networks-with-watermarking>. Accessed: 2023-06-01.
- [3] Yossi Adi, Carsten Baum, Moustapha Cisse, Benny Pinkas, and Joseph Keshet. Turning your weakness into a strength: Watermarking deep neural networks by backdooring. In *27th {USENIX} Security Symposium ({USENIX} Security 18)*, pages 1615–1631, 2018.
- [4] William Aiken, Hyoungshick Kim, and Simon S. Woo. Neural network laundering: Removing black-box backdoor watermarks from deep neural networks. *Comput. Secur.*, 106:102277, 2020.
- [5] Marco Allodi, Alberto Broggi, Domenico Giaquinto, Marco Patander, and Antonio Prioletti. Machine learning in tracking associations with stereo vision and lidar observations for an autonomous vehicle. In *2016 IEEE intelligent vehicles symposium (IV)*, pages 648–653. IEEE, 2016.
- [6] Mrinal R Bachute and Javed M Subhedar. Autonomous driving architectures: insights of machine learning and deep learning algorithms. *Machine Learning with Applications*, 6:100164, 2021.
- [7] Bryant Chen, Wilka Carvalho, Nathalie Baracaldo, Heiko Ludwig, Ben Edwards, Taesung Lee, Ian Molloy, and B. Srivastava. Detecting backdoor attacks on deep neural networks by activation clustering. *ArXiv*, abs/1811.03728, 2018.
- [8] Xinyun Chen, Wenxiao Wang, Chris Bender, Yiming Ding, Ruoxi Jia, Bo Li, and Dawn Song. Refit: a unified watermark removal framework for deep learning systems with limited data. In *Proceedings of the 2021 ACM Asia Conference on Computer and Communications Security*, pages 321–335, 2021.
- [9] Xinyun Chen, Wenxiao Wang, Yiming Ding, Chris Bender, Ruoxi Jia, Bo Li, and Dawn Song. Leveraging unlabeled data for watermark removal of deep neural networks. In *ICML workshop on Security and Privacy of Machine Learning*, pages 1–6, 2019.
- [10] Xuxi Chen, Tianlong Chen, Zhenyu Zhang, and Zhangyang Wang. You are caught stealing my winning lottery ticket! making a lottery ticket claim its ownership. *Advances in Neural Information Processing Systems*, 34:1780–1791, 2021.
- [11] Zhenzhu Chen, Shang Wang, Anmin Fu, Yansong Gao, Shui Yu, and Robert H. Deng. Linkbreaker: Breaking the backdoor-trigger link in dnns via neurons consistency check. *IEEE Transactions on Information Forensics and Security*, 17:2000–2014, 2022.
- [12] Gregory Cohen, Saeed Afshar, Jonathan Tapson, and Andre Van Schaik. Emnist: Extending mnist to handwritten letters. In *2017 international joint conference on neural networks (IJCNN)*, pages 2921–2926. IEEE, 2017.
- [13] Jeremy Cohen, Elan Rosenfeld, and Zico Kolter. Certified adversarial robustness via randomized smoothing. In *international conference on machine learning*, pages 1310–1320. PMLR, 2019.
- [14] Bitu Darvish Rouhani, Huili Chen, and Farinaz Koushanfar. Deepsigns: An end-to-end watermarking framework for ownership protection of deep neural networks. In *Proceedings of the Twenty-Fourth International Conference on Architectural Support for Programming Languages and Operating Systems*, pages 485–497, 2019.
- [15] Jacob Devlin, Ming-Wei Chang, Kenton Lee, and Kristina Toutanova. Bert: Pre-training of deep bidirectional transformers for language understanding. *arXiv preprint arXiv:1810.04805*, 2018.
- [16] Matt Fredrikson, Somesh Jha, and Thomas Ristenpart. Model inversion attacks that exploit confidence information and basic countermeasures. In *Proceedings of the 22nd ACM SIGSAC conference on computer and communications security*, pages 1322–1333, 2015.
- [17] Kathrin Grosse, Taesung Lee, Battista Biggio, Youngja Park, Michael Backes, and Ian Molloy. Backdoor smoothing: Demystifying backdoor attacks on deep neural networks. *Computers & Security*, 120:102814, 2022.
- [18] Jia Guo and Miodrag Potkonjak. Watermarking deep neural networks for embedded systems. In *2018 IEEE/ACM International Conference on Computer-Aided Design (ICCAD)*, pages 1–8. IEEE, 2018.
- [19] Shangwei Guo, Tianwei Zhang, Han Qiu, Yi Zeng, Tao Xiang, and Yang Liu. Fine-tuning is not enough: A simple yet effective watermark removal attack for dnn models. In *International Joint Conference on Artificial Intelligence*, 2020.
- [20] Abdalraouf Hassan and Ausif Mahmood. Convolutional recurrent deep learning model for sentence classification. *Ieee Access*, 6:13949–13957, 2018.
- [21] Kaiming He, Xiangyu Zhang, Shaoqing Ren, and Jian Sun. Deep residual learning for image recognition. In *Proceedings of the IEEE conference on computer vision and pattern recognition*, pages 770–778, 2016.

- [22] Gao Huang, Zhuang Liu, Laurens Van Der Maaten, and Kilian Q Weinberger. Densely connected convolutional networks. In *Proceedings of the IEEE conference on computer vision and pattern recognition*, pages 4700–4708, 2017.
- [23] Andrew Ilyas, Shibani Santurkar, Dimitris Tsipras, Logan Engstrom, Brandon Tran, and Aleksander Madry. Adversarial examples are not bugs, they are features. *Advances in neural information processing systems*, 32, 2019.
- [24] Sergey Ioffe and Christian Szegedy. Batch normalization: Accelerating deep network training by reducing internal covariate shift. In *International conference on machine learning*, pages 448–456. pmlr, 2015.
- [25] Hengrui Jia, Christopher A Choquette-Choo, Varun Chandrasekaran, and Nicolas Papernot. Entangled watermarks as a defense against model extraction. In *USENIX Security Symposium*, pages 1937–1954, 2021.
- [26] Andrew B Kahng, John Lach, William H Mangione-Smith, Stefanus Mantik, Igor L Markov, Miodrag Potkonjak, Paul Tucker, Huijuan Wang, and Gregory Wolfe. Watermarking techniques for intellectual property protection. In *Proceedings of the 35th annual Design Automation Conference*, pages 776–781, 1998.
- [27] James Kirkpatrick, Razvan Pascanu, Neil Rabinowitz, Joel Veness, Guillaume Desjardins, Andrei A Rusu, Kieran Milan, John Quan, Tiago Ramalho, Agnieszka Grabska-Barwinska, et al. Overcoming catastrophic forgetting in neural networks. *Proceedings of the national academy of sciences*, 114(13):3521–3526, 2017.
- [28] Alex Krizhevsky, Geoffrey Hinton, et al. Learning multiple layers of features from tiny images. 2009.
- [29] Erwan Le Merrer, Patrick Perez, and Gilles Trédan. Adversarial frontier stitching for remote neural network watermarking. *Neural Computing and Applications*, 32:9233–9244, 2020.
- [30] Yann LeCun, Léon Bottou, Yoshua Bengio, and Patrick Haffner. Gradient-based learning applied to document recognition. *Proceedings of the IEEE*, 86(11):2278–2324, 1998.
- [31] Yann LeCun, Corinna Cortes, and Christopher J.C. Burges. The mnist database of handwritten digits. <http://yann.lecun.com/exdb/mnist/>, 1998.
- [32] Isabell Lederer, Rudolf Mayer, and Andreas Rauber. Identifying appropriate intellectual property protection mechanisms for machine learning models: A systematization of watermarking, fingerprinting, model access, and attacks. *arXiv preprint arXiv:2304.11285*, 2023.
- [33] Suyoung Lee, Wonho Song, Suman Jana, Meeyoung Cha, and Soeul Son. Evaluating the robustness of trigger set-based watermarks embedded in deep neural networks. *IEEE Transactions on Dependable and Secure Computing*, 2022.
- [34] Huiying Li, Emily Wenger, Shawn Shan, Ben Y Zhao, and Haitao Zheng. Piracy resistant watermarks for deep neural networks. *arXiv preprint arXiv:1910.01226*, 2019.
- [35] Yige Li, Xixiang Lyu, Nodens Koren, Lingjuan Lyu, Bo Li, and Xingjun Ma. Anti-backdoor learning: Training clean models on poisoned data. *Advances in Neural Information Processing Systems*, 34:14900–14912, 2021.
- [36] Zheng Li, Chengyu Hu, Yang Zhang, and Shanqing Guo. How to prove your model belongs to you: A blind-watermark based framework to protect intellectual property of dnn. In *Proceedings of the 35th Annual Computer Security Applications Conference*, pages 126–137, 2019.
- [37] Kang Liu, Brendan Dolan-Gavitt, and Siddharth Garg. Fine-pruning: Defending against backdooring attacks on deep neural networks. In *Research in Attacks, Intrusions, and Defenses: 21st International Symposium, RAID 2018, Heraklion, Crete, Greece, September 10-12, 2018, Proceedings 21*, pages 273–294. Springer, 2018.
- [38] Xuankai Liu, Fengting Li, Bihan Wen, and Qi Li. Removing backdoor-based watermarks in neural networks with limited data. In *2020 25th International Conference on Pattern Recognition (ICPR)*, pages 10149–10156. IEEE, 2021.
- [39] Nils Lukas, Edward Jiang, Xinda Li, and Florian Kerschbaum. Sok: How robust is image classification deep neural network watermarking? In *2022 IEEE Symposium on Security and Privacy (SP)*, pages 787–804. IEEE, 2022.
- [40] Alexander Mordvintsev, Christopher Olah, and Mike Tyka. Inceptionism: Going deeper into neural networks. 2015.
- [41] Ryota Namba and Jun Sakuma. Robust watermarking of neural network with exponential weighting. In *Proceedings of the 2019 ACM Asia Conference on Computer and Communications Security*, pages 228–240, 2019.
- [42] Omkar M Parkhi, Andrea Vedaldi, and Andrew Zisserman. Deep face recognition. 2015.

- [43] Masoumeh Shafieinejad, Jiaqi Wang, Nils Lukas, and Florian Kerschbaum. On the robustness of backdoor-based watermarking in deep neural networks. *Proceedings of the 2021 ACM Workshop on Information Hiding and Multimedia Security*, 2019.
- [44] Karen Simonyan and Andrew Zisserman. Very deep convolutional networks for large-scale image recognition. *arXiv preprint arXiv:1409.1556*, 2014.
- [45] Mingjie Sun and Zico Kolter. Single image backdoor inversion via robust smoothed classifiers. In *Proceedings of the IEEE/CVF Conference on Computer Vision and Pattern Recognition*, pages 8113–8122, 2023.
- [46] Shichang Sun, Haoqi Wang, Mingfu Xue, Yushu Zhang, Jian Wang, and Weiqiang Liu. Detect and remove watermark in deep neural networks via generative adversarial networks. In Joseph K. Liu, Sokratis K. Katsikas, Weizhi Meng, Willy Susilo, and Rolly Intan, editors, *Information Security - 24th International Conference, ISC 2021, Virtual Event, November 10-12, 2021, Proceedings*, volume 13118 of *Lecture Notes in Computer Science*, pages 341–357. Springer, 2021.
- [47] Christian Szegedy, Vincent Vanhoucke, Sergey Ioffe, Jon Shlens, and Zbigniew Wojna. Rethinking the inception architecture for computer vision. In *Proceedings of the IEEE conference on computer vision and pattern recognition*, pages 2818–2826, 2016.
- [48] Yusuke Uchida, Yuki Nagai, Shigeyuki Sakazawa, and Shin’ichi Satoh. Embedding watermarks into deep neural networks. In *Proceedings of the 2017 ACM on international conference on multimedia retrieval*, pages 269–277, 2017.
- [49] Laurens Van der Maaten and Geoffrey Hinton. Visualizing data using t-sne. *Journal of machine learning research*, 9(11), 2008.
- [50] Bolun Wang, Yuanshun Yao, Shawn Shan, Huiying Li, Bimal Viswanath, Haitao Zheng, and Ben Y Zhao. Neural cleanse: Identifying and mitigating backdoor attacks in neural networks. In *2019 IEEE Symposium on Security and Privacy (SP)*, pages 707–723. IEEE, 2019.
- [51] Tianhao Wang and Florian Kerschbaum. Riga: Covert and robust white-box watermarking of deep neural networks. In *Proceedings of the Web Conference 2021*, pages 993–1004, 2021.
- [52] Yifan Yan, Xudong Pan, Mi Zhang, and Min Yang. Rethinking white-box watermarks on deep learning models under neural structural obfuscation. In *32th USENIX security symposium (USENIX Security 23)*, 2023.
- [53] Ziqi Yang, Hung Dang, and Ee-Chien Chang. Effectiveness of distillation attack and countermeasure on neural network watermarking. *ArXiv*, abs/1906.06046, 2019.
- [54] Hongxu Yin, Pavlo Molchanov, Jose M Alvarez, Zhizhong Li, Arun Mallya, Derek Hoiem, Niraj K Jha, and Jan Kautz. Dreaming to distill: Data-free knowledge transfer via deepinversion. In *Proceedings of the IEEE/CVF Conference on Computer Vision and Pattern Recognition*, pages 8715–8724, 2020.
- [55] Youngsik Yoon, Jinhwan Nam, Hyojeong Yun, Dongwoo Kim, and Jungseul Ok. Few-shot unlearning by model inversion. *arXiv preprint arXiv:2205.15567*, 2022.
- [56] Jialong Zhang, Zhongshu Gu, Jiyong Jang, Hui Wu, Marc Ph Stoecklin, Heqing Huang, and Ian Molloy. Protecting intellectual property of deep neural networks with watermarking. In *Proceedings of the 2018 on Asia Conference on Computer and Communications Security*, pages 159–172, 2018.
- [57] Jianpeng Zhang, Yutong Xie, Qi Wu, and Yong Xia. Medical image classification using synergic deep learning. *Medical image analysis*, 54:10–19, 2019.
- [58] Qi Zhong, Leo Yu Zhang, Shengshan Hu, Longxiang Gao, Jun Zhang, and Yang Xiang. Attention distraction: Watermark removal through continual learning with selective forgetting. *2022 IEEE International Conference on Multimedia and Expo (ICME)*, pages 1–6, 2022.

## A Omitted Details of MIRA

### A.1 Classical Natural Image Priors

Specifically, we incorporate two regularization terms  $\mathcal{R}_{\ell_2}(\cdot)$  and  $\mathcal{R}_{\ell_v}(\cdot)$ , as demonstrated in [40], which correspond to  $\ell_2$  distance and total variation, to steer the optimized samples away from unrealistic ones:

$$\mathcal{R}_{\ell_2}(B) = \sum_{\hat{x}_i \in B} \|\hat{x}_i\|_2^2, \quad (8)$$

$$\mathcal{R}_{\ell_v}(B) = \sum_{\hat{x}_i \in B} \sum_{(j,k)} \sum_{(j',k') \in \delta(j,k)} \|\hat{x}_{i(j,k)} - \hat{x}_{i(j',k')}\|_2^2, \quad (9)$$

where  $\delta(j,k)$  indicates a set of pixels adjacent to the pixel at  $(j,k)$  in the image  $\hat{x}_i$ .

### A.2 Splitting Recovered Samples

The detailed pipeline to class-wise split the recovered samples is shown in Alg. 1.



---

**Algorithm 1** Split recovered samples.

---

**Input:** target model  $f_w$  and its  $l$ -th layer to analyse, recovered samples  $\{B_c\}_*$ , saliency ratio  $\beta$ , split ratio  $\gamma$ .

**Output:** proxy watermark samples  $\{B_{c,wmk}\}_*$ , proxy normal samples  $\{B_{c,nor}\}_*$ .

```
1:  $M \leftarrow$  samples' size of each  $B_c$  in  $\{B_c\}_*$ ,  
    $D \leftarrow$  neurons' size of the  $l$ -th layer  
2:  $\{B_{c,wmk}\}_* \leftarrow \{\}, \{B_{c,nor}\}_* \leftarrow \{\}$   
3: for batch  $B_c$  in  $\{B_c\}_*$  do  
4:   Forward propagate and extract activation of the  $l$ -th  
   layer  $act = f_{w(l)}(B_c)$   
   /* Find salient neurons */  
5:    $Impt \leftarrow \{\}$   
6:   for neuron  $j = 0, 1, \dots, D - 1$  do  
7:      $Impt[j] \leftarrow \frac{\mu_j}{\sigma_j}$   
8:   end for  
9:    $sorted\_neurons \leftarrow \text{argsort}(Impt)$   
10:   $salient\_neurons \leftarrow sorted\_neurons[: \beta \times D]$   
   /* Split recovered batch  $B_c$  */  
11:   $Contribution \leftarrow \{\}$   
12:  for sample  $\hat{x}_i$  in  $B_c$  do  
13:     $Contribution[i] \leftarrow \text{sum}(act[i, salient\_neurons])$   
14:  end for  
15:   $sorted\_samples \leftarrow \text{argsort}(Contribution)$   
16:   $proxy\_wmk \leftarrow sorted\_samples[: \gamma \times M],$   
    $proxy\_nor \leftarrow sorted\_samples[\gamma \times M :]$   
17:   $B_{c,wmk} \leftarrow B_c[proxy\_wmk],$   
    $B_{c,nor} \leftarrow B_c[proxy\_nor]$   
18:  Append split data  $B_{c,wmk}$  and  $B_{c,nor}$  to  $\{B_{c,wmk}\}_*$  and  
    $\{B_{c,nor}\}_*$  respectively  
19: end for  
20: return  $\{B_{c,wmk}\}_*, \{B_{c,nor}\}_*$ 
```

---

## B Omitted Details in Experiments

### B.1 More Backgrounds on Existing Black-box Model Watermarking Schemes

Our evaluation covers ten existing black-box DNN watermarks, which are categorized as *fixed-class watermarks* (i.e., all the watermark data are paired with the identical target class), and *non-fixed-class watermarks* (i.e., each watermark data is paired with its own target class).

- *Fixed-class watermarks*: (1) **Content**, (2) **Noise**, (3) **Unrelated** [56]. *Content* and *Noise* watermarks draw normal samples from a source class and apply watermark patterns, which are text shapes and random noises respectively, as watermark data. *Unrelated* watermark draws samples from another dataset. All these selected watermark data are annotated with one fixed target class. (4) **Piracy** [34] modifies the values of certain pixels in an image to extreme maximum or minimum values as the trigger, which is then mapped

to a fixed class. The position of these pixels and the target class are determined by a signature provided by the user. (5) **EWE** [25] selects samples from a source class, adds square patterns and annotates with a fixed target class. During training, EWE enforces the model to learn entangled features between watermark samples and normal samples of the target class.

- *Non-fixed-class watermarks*: (6) **Adi** [3] leverages a set of abstract out-of-distribution images as watermark data and annotates them randomly. (7) **AFS** [29] generates adversarial examples near the classification boundary of a normally trained model and annotates them with the ground-truth label. The model is then finetuned with these samples added to the training set. (8) **EW** [41] selects normal samples and annotates them with random labels except the ground-truth. During embedding, a normally trained model is applied with an exponential weight operator layer-wise, and then finetuned with watermark samples added to the training set. (9) **Blind** [36] takes ordinary samples and exclusive logos as inputs, uses an encoder to generate watermarks that are almost indistinguishable from the original samples, and uses a discriminator to assist in training. All watermarks are labeled as a fixed class. (10) **Mark** [18] modifies a portion of the dataset based on the user's signature. The pixel values at specific positions of each image are modified to extreme values according to the signature, and the label of each image is mapped to one of the remaining labels in a specific way based on the signature..

### B.2 Implementations of the Target Watermark Schemes

We implement the target black-box watermark schemes based on the open-source watermark framework provided by Lederer et al. [32]. For those watermarks not included in this framework (e.g., *EWE* [25] and *Blind* [36]), we reproduce them by referring to another well-known repository [39] and use the hyper-parameters suggested in the original papers. For *Piracy* [34] and *Blind* [36], we set the size for watermark data as 1% of the clean training set, following their papers. For other black-box watermarks, the size of watermark data is set to 100.

### B.3 Performance of Watermarked Models

The performance of the well-trained DNN model protected by ten different black-box watermarks on three benchmark dataset is shown in Table B.1.

### B.4 Details of Baseline Removal Attacks

Here we provide some implementation details of the baseline removal attacks. For the Pruning attack, we set the weight prune ratio to 80%. For the *Fine-pruning* attack, we set the

Table B.1: The performance of the target watermarked models on three datasets. The threshold is estimated on 20 null models as suggested by Lukas et al. [39]

| Watermarks       | MNIST     |        |           | CIFAR-10  |        |           | CIFAR-100 |        |           |
|------------------|-----------|--------|-----------|-----------|--------|-----------|-----------|--------|-----------|
|                  | Clean acc | WM acc | Threshold | Clean acc | WM acc | Threshold | Clean acc | WM acc | Threshold |
| <b>Content</b>   | 99.08     | 100    | 0.0083    | 93.77     | 100    | 0.1044    | 76.27     | 100    | 0.0244    |
| <b>Noise</b>     | 99        | 100    | 0.1057    | 94.13     | 100    | 0.4697    | 76.67     | 100    | 0.0151    |
| <b>Unrelated</b> | 98.94     | 100    | 0.088     | 93.65     | 100    | 0.0931    | 75.93     | 100    | 0.0305    |
| <b>Piracy</b>    | 99.22     | 100    | 0.2807    | 93.31     | 100    | 0.1966    | 73.69     | 100    | 0.1672    |
| <b>EWE</b>       | 98.86     | 100    | 0.0025    | 93.97     | 100    | 0.045     | 67.73     | 100    | 0.0059    |
| <b>Adi</b>       | 98.82     | 100    | 0.149     | 93.91     | 100    | 0.1425    | 75.56     | 100    | 0.0176    |
| <b>AFS</b>       | 98.73     | 100    | 0.1506    | 92.96     | 100    | 0.2103    | 65.76     | 100    | 0.0813    |
| <b>EW</b>        | 98.55     | 100    | 0.0025    | 92.89     | 100    | 0.1335    | 75.98     | 100    | 0.0088    |
| <b>Blind</b>     | 98.64     | 100    | 0.1432    | 91.18     | 100    | 0.1452    | 67.22     | 100    | 0.0266    |
| <b>Mark</b>      | 98.57     | 100    | 0.0025    | 93.97     | 100    | 0.1381    | 65.25     | 100    | 0.0125    |

Table C.2: Comparison of removal attacks against black-box watermarks under the in-distribution setting on MNIST.  $x / y$  denotes the clean accuracy / rescaled watermark accuracy.

| Attacks               | Content      | Noise        | Unrelated    | Piracy       | EWE          | Adi          | AFS          | EW           | Blind        | Mark         |
|-----------------------|--------------|--------------|--------------|--------------|--------------|--------------|--------------|--------------|--------------|--------------|
| None                  | 99.1 / 100.0 | 99.0 / 100.0 | 98.9 / 100.0 | 99.2 / 100.0 | 98.9 / 100.0 | 98.8 / 100.0 | 98.7 / 100.0 | 98.5 / 100.0 | 98.6 / 100.0 | 98.6 / 100.0 |
| <i>Fine-pruning</i>   | 96.6 / 53.6  | 97.0 / 47.4  | 97.7 / 100.0 | 98.4 / 75.0  | 97.8 / 100.0 | 96.0 / 52.4  | 95.6 / 50.0  | 97.4 / 54.4  | 97.3 / 49.8  | 96.0 / 53.4  |
| <i>Finetuning</i>     | 97.7 / 60.7  | 97.2 / 45.2  | 97.4 / 99.5  | 99.1 / 100.0 | 97.4 / 87.0  | 95.3 / 48.3  | 97.3 / 58.8  | 95.3 / 54.4  | 95.9 / 49.2  | 95.8 / 52.9  |
| <i>Regularization</i> | 97.4 / 50.6  | 97.6 / 45.8  | 97.2 / 53.9  | 97.3 / 41.6  | 97.7 / 51.4  | 97.4 / 55.3  | 97.0 / 50.6  | 95.7 / 54.4  | 95.9 / 51.0  | 96.0 / 53.9  |
| <i>Distraction</i>    | 90.4 / 52.6  | 87.3 / 44.6  | 90.8 / 45.7  | 99.2 / 100.0 | 95.0 / 49.9  | 97.9 / 55.9  | 85.8 / 50.6  | 85.5 / 55.9  | 94.4 / 51.6  | 93.9 / 54.4  |
| <i>Laundering</i>     | 97.0 / 51.6  | 97.7 / 46.9  | 96.0 / 45.2  | 98.6 / 36.7  | 96.0 / 53.4  | 95.4 / 48.3  | 96.6 / 50.0  | 95.8 / 55.4  | 96.9 / 49.8  | 96.2 / 53.4  |
| MIRA (Basic)          | 96.7 / 50.6  | 96.7 / 44.6  | 93.8 / 45.2  | 96.3 / 37.4  | 97.1 / 49.9  | 96.7 / 49.5  | 96.9 / 46.4  | 95.9 / 53.9  | 96.1 / 49.2  | 96.9 / 52.9  |
| MIRA (Improved)       | 96.7 / 50.6  | 96.7 / 44.6  | 93.8 / 45.2  | 96.3 / 37.4  | 97.1 / 49.9  | 96.7 / 49.5  | 96.9 / 46.4  | 95.9 / 53.9  | 96.1 / 49.2  | 96.9 / 52.9  |

Table C.3: Comparison of removal attacks against black-box watermarks under the in-distribution setting on CIFAR-100.

| Attacks               | Content      | Noise        | Unrelated    | Piracy       | EWE          | Adi          | AFS          | EW           | Blind        | Mark         |
|-----------------------|--------------|--------------|--------------|--------------|--------------|--------------|--------------|--------------|--------------|--------------|
| None                  | 76.3 / 100.0 | 76.7 / 100.0 | 75.9 / 100.0 | 73.7 / 100.0 | 67.7 / 100.0 | 75.6 / 100.0 | 65.8 / 100.0 | 76.0 / 100.0 | 67.2 / 100.0 | 65.2 / 100.0 |
| <i>Fine-pruning</i>   | 56.3 / 53.9  | 58.6 / 54.3  | 58.4 / 48.4  | 7.6 / 40.0   | 63.3 / 95.5  | 57.5 / 56.2  | 51.2 / 70.6  | 52.6 / 61.7  | 10.6 / 49.1  | 51.3 / 61.5  |
| <i>Finetuning</i>     | 67.3 / 100.0 | 68.5 / 100.0 | 67.9 / 100.0 | 12.5 / 40.0  | 60.1 / 99.0  | 69.5 / 99.5  | 63.2 / 98.9  | 68.5 / 96.5  | 31.2 / 59.4  | 63.4 / 98.0  |
| <i>Regularization</i> | 58.2 / 100.0 | 59.2 / 100.0 | 60.4 / 100.0 | 60.5 / 40.0  | 25.9 / 49.7  | 57.1 / 100.0 | 31.9 / 69.0  | 59.5 / 96.5  | 36.1 / 70.7  | 34.7 / 52.4  |
| <i>Distraction</i>    | 56.1 / 48.7  | 50.1 / 49.2  | 60.9 / 48.4  | 58.7 / 46.0  | 64.7 / 100.0 | 59.8 / 51.1  | 63.7 / 99.5  | 56.6 / 50.6  | 27.0 / 49.1  | 64.4 / 85.8  |
| <i>Laundering</i>     | 67.6 / 49.8  | 68.0 / 49.2  | 67.8 / 48.4  | 46.7 / 40.6  | 47.3 / 49.7  | 58.9 / 71.0  | 60.1 / 96.7  | 66.9 / 93.9  | 33.3 / 49.1  | 62.1 / 91.9  |
| MIRA (Basic)          | 72.6 / 48.7  | 63.2 / 57.9  | 63.0 / 55.6  | 65.8 / 44.8  | 64.5 / 49.7  | 62.1 / 57.2  | 65.2 / 57.5  | 61.2 / 57.1  | 54.5 / 58.4  | 64.0 / 60.5  |
| MIRA (Improved)       | 75.1 / 48.7  | 73.9 / 50.2  | 73.1 / 53.1  | 71.0 / 41.8  | 67.1 / 49.7  | 64.8 / 60.3  | 65.4 / 54.8  | 62.8 / 59.6  | 65.1 / 55.8  | 64.5 / 58.5  |

neuron prune ratio to 20%. For the *Finetuning* attack, we start with a learning rate of 0.05 as in [9], followed by a gradually decreasing learning rate schedule. For the Regularization attack, we reproduce it based on an open-source repository<sup>2</sup>. For the *Distraction* attack, we strictly follow the original paper [58]. For the *Laundering* attack, we follow the main method in [4] and implement it with a certain watermark knowledge. We use the original labels for watermarks using non-OOD data, and least-likely labels for watermarks using OOD data.

## C More Experiment Results

### C.1 Attack Results on MNIST

Note that MNIST is a relatively simple task, and the LeNet-5 [30] structure we select has no batch normalization layers. In this case, we simply set the term  $\mathcal{R}_{bn}(B) = 0$  during watermark recovering. Both the basic and improved MIRA still perform well, illustrating the generality of our methods. We select 1000 samples for the in-distribution setting, and 2000 samples from EMNIST [12] for the transfer setting.

### C.2 Attack Results on CIFAR-100

For the CIFAR-100 dataset, we select 1000 samples for the in-distribution setting, and 2000 samples from CIFAR-10 for the transfer setting.

<sup>2</sup><https://github.com/CodeSubmission642/WatermarkRobustness>

Table C.4: Comparison of removal attacks against black-box watermarks under the transfer setting on MNIST.

| Attacks         | Content      | Noise        | Unrelated    | Piracy       | EWE          | Adi          | AFS          | EW           | Blind        | Mark         |
|-----------------|--------------|--------------|--------------|--------------|--------------|--------------|--------------|--------------|--------------|--------------|
| None            | 99.1 / 100.0 | 99.0 / 100.0 | 98.9 / 100.0 | 99.2 / 100.0 | 98.9 / 100.0 | 98.8 / 100.0 | 98.7 / 100.0 | 98.5 / 100.0 | 98.6 / 100.0 | 98.6 / 100.0 |
| Regularization  | 73.1 / 75.8  | 61.0 / 60.9  | 65.5 / 99.5  | 67.8 / 91.0  | 77.8 / 49.9  | 72.0 / 58.9  | 62.6 / 58.2  | 72.2 / 59.9  | 80.3 / 53.9  | 74.7 / 57.4  |
| Distraction     | 85.9 / 52.1  | 91.8 / 44.1  | 96.2 / 81.4  | 99.2 / 100.0 | 98.9 / 100.0 | 95.9 / 61.8  | 87.5 / 60.0  | 88.2 / 53.9  | 98.5 / 90.1  | 94.8 / 62.4  |
| MIRA (Basic)    | 83.2 / 54.1  | 96.3 / 46.3  | 95.4 / 51.2  | 96.9 / 42.3  | 97.0 / 53.4  | 94.8 / 61.2  | 90.9 / 55.3  | 90.3 / 75.4  | 91.8 / 64.4  | 90.8 / 84.0  |
| MIRA (Improved) | 96.8 / 53.1  | 98.6 / 44.6  | 97.3 / 45.2  | 98.1 / 36.0  | 97.9 / 49.9  | 95.8 / 60.6  | 90.6 / 51.1  | 92.3 / 62.4  | 91.9 / 62.7  | 91.1 / 61.9  |

Table C.5: Comparison of removal attacks against black-box watermarks under the transfer setting on CIFAR-100.

| Attacks         | Content      | Noise        | Unrelated    | Piracy       | EWE          | Adi          | AFS          | EW           | Blind        | Mark         |
|-----------------|--------------|--------------|--------------|--------------|--------------|--------------|--------------|--------------|--------------|--------------|
| None            | 76.3 / 100.0 | 76.7 / 100.0 | 75.9 / 100.0 | 73.7 / 100.0 | 67.7 / 100.0 | 75.6 / 100.0 | 65.8 / 100.0 | 76.0 / 100.0 | 67.2 / 100.0 | 65.2 / 100.0 |
| Regularization  | 59.3 / 100.0 | 53.9 / 100.0 | 52.6 / 100.0 | 48.4 / 100.0 | 42.3 / 49.7  | 60.3 / 100.0 | 52.2 / 90.2  | 57.1 / 95.5  | 43.8 / 88.2  | 49.3 / 52.4  |
| Distraction     | 76.3 / 90.3  | 76.4 / 100.0 | 76.0 / 99.5  | 72.3 / 52.6  | 64.9 / 100.0 | 56.3 / 50.1  | 63.1 / 97.8  | 59.4 / 57.6  | 66.7 / 98.5  | 63.8 / 77.7  |
| MIRA (Basic)    | 72.7 / 48.7  | 56.6 / 51.3  | 62.3 / 58.2  | 64.1 / 50.2  | 56.2 / 59.8  | 59.1 / 58.3  | 58.4 / 54.8  | 59.5 / 59.1  | 55.7 / 54.8  | 55.4 / 60.0  |
| MIRA (Improved) | 74.0 / 48.7  | 75.2 / 49.7  | 70.0 / 58.2  | 71.0 / 44.8  | 62.2 / 59.3  | 55.1 / 52.7  | 58.8 / 49.9  | 61.9 / 58.6  | 56.1 / 54.3  | 61.1 / 58.5  |

Table C.6: Comparison of removal attacks against black-box watermarks under the data-free setting on MNIST.

| Attacks         | Content      | Noise        | Unrelated    | Piracy       | EWE          |
|-----------------|--------------|--------------|--------------|--------------|--------------|
| None            | 99.1 / 100.0 | 99.0 / 100.0 | 98.9 / 100.0 | 99.2 / 100.0 | 98.9 / 100.0 |
| Pruning         | 98.9 / 100.0 | 98.3 / 100.0 | 98.8 / 100.0 | 99.1 / 100.0 | 98.5 / 99.5  |
| MIRA (Improved) | 93.2 / 49.6  | 97.8 / 44.1  | 89.3 / 47.9  | 97.3 / 36.0  | 94.5 / 49.9  |

Table C.7: Comparison of removal attacks against black-box watermarks under the data-free setting on CIFAR-100.

| Attacks         | Content      | Noise        | Unrelated    | Piracy       | EWE          |
|-----------------|--------------|--------------|--------------|--------------|--------------|
| None            | 76.3 / 100.0 | 76.7 / 100.0 | 75.9 / 100.0 | 73.7 / 100.0 | 67.7 / 100.0 |
| Pruning         | 66.4 / 100.0 | 66.9 / 100.0 | 58.7 / 100.0 | 26.7 / 40.0  | 60.2 / 100.0 |
| MIRA (Improved) | 70.0 / 50.8  | 72.2 / 51.8  | 61.1 / 58.7  | 71.1 / 41.8  | 57.5 / 60.3  |

### C.3 Comparison with Other Recovering Methods

**Visual Differences.** Fig.C.1 visualizes the recovered samples of MIRA and DeepInversion. Compared with *Content* and *EWE*, our MIRA can recover samples with patterns similar to the real watermark data, such as the dark text shapes for *Content*, and white patches for *EWE*. In contrast, DeepInversion tends to produce more realistic images belonging to class 6 (i.e., "frogs" for CIFAR-10). Note that the black borderlines in its recovered samples for *Content* are simply evidences of the random cropping augmentations usually introduced during training, rather than the actual text shapes of watermark data. With regard to *Adi*, our MIRA can also recover samples with more evident and colorful fringing than DeepInversion. These visual differences demonstrate the effectiveness of our aggressive inversion scheme.

**Attack Performance Differences.** For DeepInversion, unlearning its inverted samples from class 6 is ineffective in removing *Content* and *EWE* watermarks, which aligns with the previous visual observations. This is mainly because the BN statistics of the watermark data might diffuse into other classes during its random-class inversion scheme. The recovered samples are therefore more representative of the normal

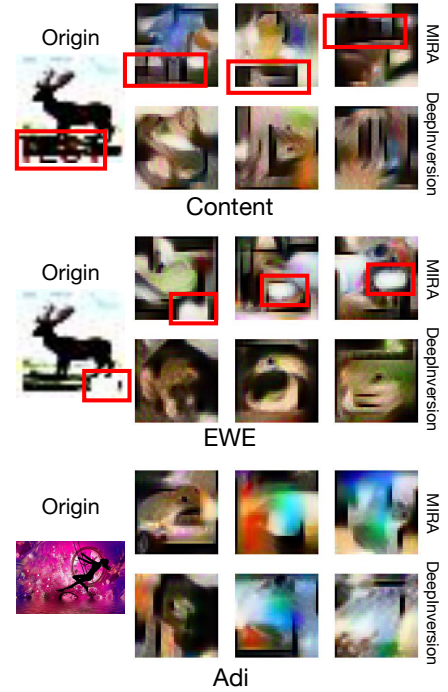


Figure C.1: Comparison of recovered samples using MIRA and DeepInversion from class 6 on CIFAR-10. The three images on the left are the real watermark samples, the upper three images in each subfigure are recovered using MIRA, and the lower three ones are recovered using DeepInversion.

data, but less informative of the watermark data, for which unlearning on them incurs a larger utility loss, compared with our MIRA.

*NeuralCleanse* is effective against *Content*, possibly because the poisoned samples happen to occupy the salient neurons of the real watermark data. However, it is ineffective against *EWE* and *Adi*, as their watermark data are better entangled with the normal data, and the generated triggers cannot provide valid coverage of the real watermark data.